学位論文(要約)

Oxidation-promoted interfacial synthesis of bis(diimino)metal
coordination nanosheets and their properties

(酸化的界面反応によるビス(ジイミノ) 金属
錯体ナノシートの合成と性質)

平成 29 年 12 月　博士（理学）申請

東京大学大学院理学系研究科

化学専攻

潘佳涵

Phua Jia Han Eunice

Oxidation-promoted interfacial synthesis of bis(diimino)metal coordination nanosheets and their properties

A dissertation
submitted in partial fulfilment of
the requirements for the degree
of
Doctor of Philosophy
in
Chemistry
(censored)

by

Phua Jia Han Eunice

Graduate School of Science
The University of Tokyo
December 2017

ABSTRACT

In this dissertation, amino-based π-conjugated nickel complex nanosheets were synthesized using a bottom up synthetic method. The dissertation opens with the background of such coordination nanosheets or CONASHs, the potential of such sheets and the aim of the research.

Nickel(II) coordination nanosheets of various thicknesses have been successfully synthesized using the hexaaminobenzene (**HAB**) ligand with an optimized oxygen-assisted interfacial reaction to form **NiDI**. Chapter 2 focuses on the chemical method which uses reactants in a homogeneous aqueous solution first set up in the glove box. The slow exposure to atmospheric oxygen is the crux for the high crystallinity of the sheets formed. With this gas/liquid interfacial reaction method, large centimetre-scale **NiDI** nanosheets with high crystallinity visible to the naked eye can be obtained.

Another synthetic method using electrochemical oxidation, which produces the **NiDI** nanosheet directly on an electrode surface, was also developed. Chapter 3 of this dissertation explores about the synthesis, characterization, as well as the investigations of the electrochemically synthesized **NiDI** nanosheet. This electrochemical method enables a more controllable growth of the nanosheet as compared to the gas-liquid interfacial reaction as the degree of oxidation can be precisely adjusted.

Using the same chemical method which utilizes ambient oxygen for synthesis, new systems were investigated by changing the nickel ion source to other metal sources. New systems involving Group 10 elements were investigated and characterized. These findings and a discussion of the new systems formed are given in Chapter 4.

The concluding remarks and the research perspectives are then given in Chapter 5, the final chapter.

TABLE OF CONTENTS

This chapter is not published because it is scheduled to be published in journals or other publications within five years.

Chapter 1

INTRODUCTION

1 INTRODUCTION

1.1. Coordination Compounds and their Dimensionalities

Coordination compounds are made up of metallic atoms or ions which are surrounded by ions or bound molecules, known as ligands, that are usually organic components. Depending on the types of bridging ligands, some of these coordination compounds can form extended structures by repeating the coordination entities, while others would form metal clusters or discrete single molecular compounds. This generally depends on the number of available coordinating sites that the particular ligand contains and how many of these sites are coordinated to the metal centres. These possibilities and the resultant coordination compounds can form different dimensions such as a zero-dimensional complex, a one-dimensional wire, two-dimensional sheets or three-dimensional lattices. Coordination compounds are thus able to be classified by the additional property of dimensionality.

One example of a zero-dimensional coordination compound would be the metal clusters or complexes which exist as discrete molecules and do not extend outwards. The ligands of the metal clusters usually only have a single binding site which do not allow any additional coordinations to other metal ions. These compounds are hence determined to be zero dimensional *i.e.* discrete coordination complexes. On the other hand, a structure can have higher dimensionalities when its array of bridging ligands allows extension in space. The eventual dimension of the compound depends on the number of directions in space the array extends in. If we take the x-axis to be the primary axis, a one-dimensional structure extends only in one axis in a straight line (along the x axis); a two-dimensional structure extends in a plane of two directions, both x and y axes); and a three-dimensional structure extends in all three directions (x, y, and z axes).[1] This leads to the formation of metal complex wires (1D), two-dimensional metal coordination sheets and three dimensional framework materials, also known as Metal Organic Frameworks or MOFs.[2] Fig. 1-1 shows some examples of the various dimensions of the possible coordination compounds.
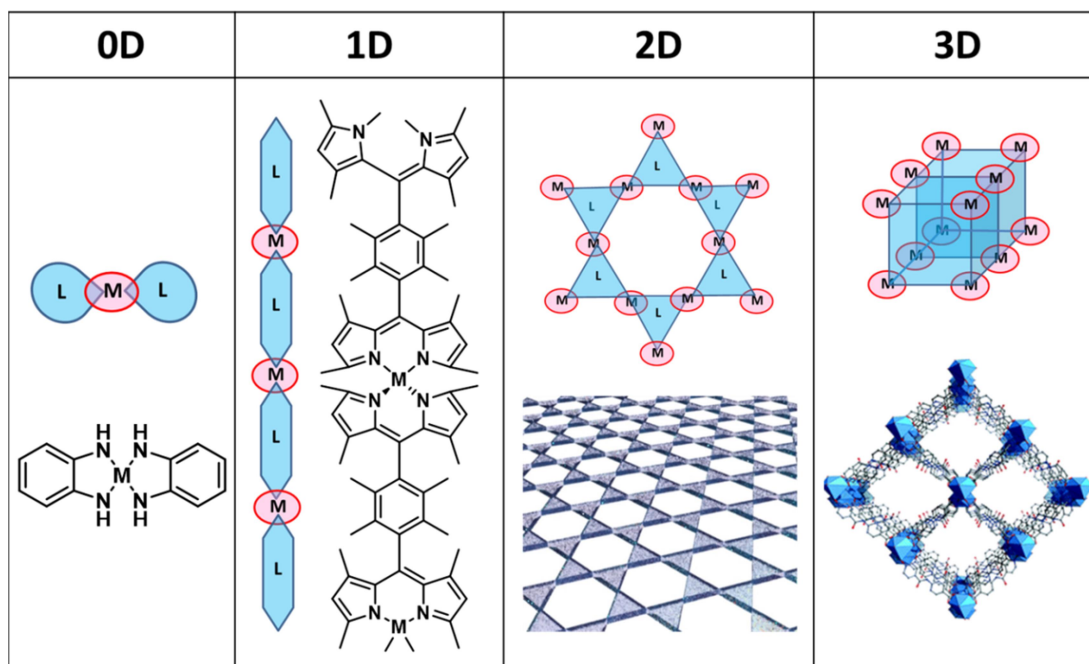
Fig. 1-1: Possible dimensionalities of coordination compounds and their examples. M represents metal ions while L represents ligands.

For the formation of 1D structure such as one-dimensional wires, the ligands usually contain coordination sites along the main axis. For the higher dimensionalities, the ligands (the linkers) are typically with the potential to form polydentate organic components, whilst the central metal ions (the node) contain multiple coordination sites along different spatial axes, which enables infinite extensions in those directions. It is also possible to form higher dimensionality compounds by having repeating units of their corresponding compounds of lower dimensions. For example, a two-dimensional sheet could be made of wires lined up in a plane, or three dimensional materials can consist of multiple two-dimensional sheets stacked together. Such a node-and-linker approach to creating such coordination polymers is essential when designing new two- and three-dimensional materials. Depending on the arrangement and composition of each subcomponent/building block, different synthetic strategies can be employed which can affect the overall obtained yield of the compound.

Various coordination compounds with different dimensionalities have been designed and synthesized over the years. Many of such uncommon and tuneable structures are necessary building blocks for the discovery and construction of various

functional supramolecular devices or materials.[3] The preparation of these different types and dimensionalities of coordination compounds is wide-ranging. They include molecular self-assembly and the crystallization of a metal salt with a ligand, where the mechanisms of crystal engineering and supramolecular chemistry are relevant.

Molecular self-assembly based on the principle of crystal engineering has proven to be an efficient approach for the formation of 1D, 2D and 3D framework materials. The research on the chemistry of these coordination compounds in different dimensionalities has been developing rapidly for the last twenty years. This is especially so for the three dimensional MOFs, due to potential applications such as catalysis, gas storage, separations, drug delivery, magnetism, fluorescence, non-linear optics and photonics.[4] This interest is also owing to their coordination possibilities and relative ease of synthesis, typically attributable to their relative stability.

1.2.   Two-dimensional Compounds

In recent years, the synthesis and study of the physicochemical properties of two-dimensional (2D) metal-ligand coordination compounds have been the focus of many material scientists, with particular interest on the investigation of the interaction between the d orbitals of the metal ions with the π orbitals of the ligands. Such 2D materials have similar functions and applications similar to that of their three-dimensional (3D) compounds and exhibit unusual physical properties due to the quantum size effect associated with their ultra-thin structure.[5] The electronic structure of a material is affected when one or more of its dimensions approach interatomic distances, like when the thicknesses of 2D materials are decreased.

Graphene, which is a 2D single layer of carbon atoms, has been in the spotlight in the past two decades, becoming one of the most famous two-dimensional nanomaterials (Fig. 1-2).[6] With a backbone of sp^2-bonded carbon atoms, graphene is a π-conjugated system with one-atom-thick planar sheets of carbon atoms that are densely packed in a honeycomb structure. It is typically obtained from its three-dimensional layered structure of graphite and has shown exceptional electronic, optical, thermal, and mechanical properties.[7] These properties make graphene promising for many applications, such as fuel cells, photovoltaic devices and biosensors.[8] Some of its possible synthetic methods would be discussed later.
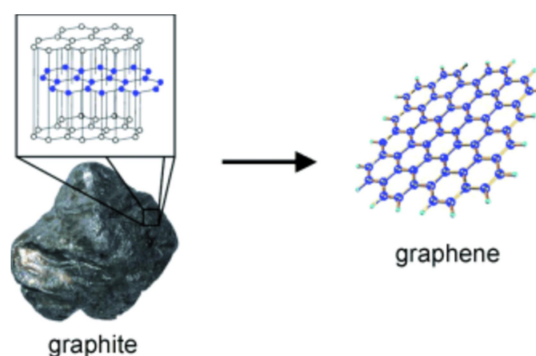
Fig. 1-2: The most famous 2D material: Graphene, obtained from graphite.[6c]

Unlike graphene which is only made up of carbon atoms, there are also many other types of two-dimensional compounds which are made of a combination of

different elements. Some of the examples include purely inorganic or organic based compounds such as metal carbides (MAX phase), graphitic carbon nitride (g-C_3N_4), hexagonal boron nitride (h-BN), black phosphorus (BP), or two-dimensional covalent organic frameworks.[9] Even with different components, the thin structures and the resulting quantum size effect of these two-dimensional compounds still retain the possibility that they may have many interesting properties worth exploring.

In addition, another highly researched area is the chemical modifications of graphene-like materials. The addition or doping of other elements not only alters its electronic properties, but also improves the solubility of graphene in organic solvents.[10] With the increased solubility, the graphene-based materials become more viable since they can be easily functionalized and conjugated with other materials such as organic polymers, metallic nanoparticles and inorganic nanosheets.[11] Such modifications further enable the tuning of the physical and electronic properties of graphene and increase the range of potential applicability of these materials as electrodes or solar devices.[12]

Other than organic materials and graphene-based nanosheets, 2D coordination compounds containing metallic atoms or ions have also been investigated. Some examples of these compounds include layered transition metal oxides (TMOs; $Cs_{0.67}Ti_{1.83}O_4$, $K_{0.45}MnO_2$, $Ca_2Nb_3O_{10}$, VO_2, MoO_3, etc.), layered double hydroxides (LDHs) or layered transition metal dichalcogenides (TMDs; MoS_2, SnS_2, WS_2, $MoSe_2$, WSe_2, etc.). These compounds have been actively explored for their ferroelectricity, semi-conductivity, photoluminescence characteristics and their use for various applications (Fig. 1-3).[13]

Many of the aforementioned 2D coordination films and graphene have the commonality of being synthesized using a top-down method of exfoliation from their layered 3D bulk material. Using such a top-down approach enables the formation of individual or thinner layers of the desired 2D compounds. There are numerous top-down synthetic methods to isolate 2D films, with the 'Scotch tape' exfoliation method, and the electrochemical method by intercalation of the layers using ions, being the most preferred and commonly employed methods (Fig. 1-4).
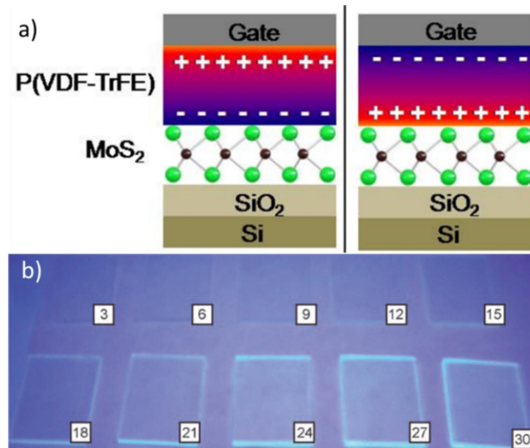
Fig. 1-3: Some examples of applications for 2D films: (a) Metal sulfides used in a transistor. Adapted with permission from ref. 13a. Copyright (2012) John Wiley and Sons. (b) Photoluminescence of metal oxides gets stronger with the increased number of layers. Reprinted with permission from ref. 13a. Copyright (2009) John Wiley and Sons.
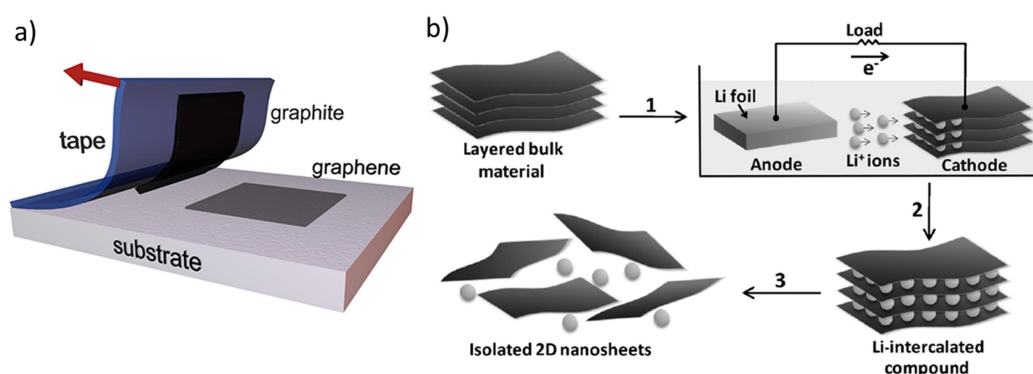

Fig. 1-4: Some examples of top-down method synthesis for 2D films: (a) Scotch tape method for graphene;[14a] (b) Electrochemical lithiation process. Adapted with permission from ref. 13b. Copyright (2011) John Wiley and Sons.

These types of top-down methods have been widely used for the syntheses of 2D films because of their relative simplicity and reproducibility. The main synthetic disadvantage, however, is that the structure of the derived 2D material is determined by the elemental composition and structure of the main bulk starting material. In other words, the syntheses of the 2D films are confined by the types and the structures of the bulk materials available, and are inherently limiting the variety of 2D compounds that can be synthesized. Furthermore, not all 3D compounds can be used to synthesize their corresponding 2D films; only the layered type structures are available. To overcome this problem, and to introduce flexibility and variety in the 2D materials that can be obtained, a different synthetic strategy should be considered.

1.3.   Bottom-up Coordination Compounds

One possible synthetic solution to the aforementioned challenge is the bottom-up approach. This refers to the synthesis of materials starting from a smaller dimensionality (zero dimension or one dimension), to form materials of higher dimensionalities (Fig. 1-5).[14b] These two terms were first used in nanotechnology to describe the methods of creating new nanomaterials.[15]
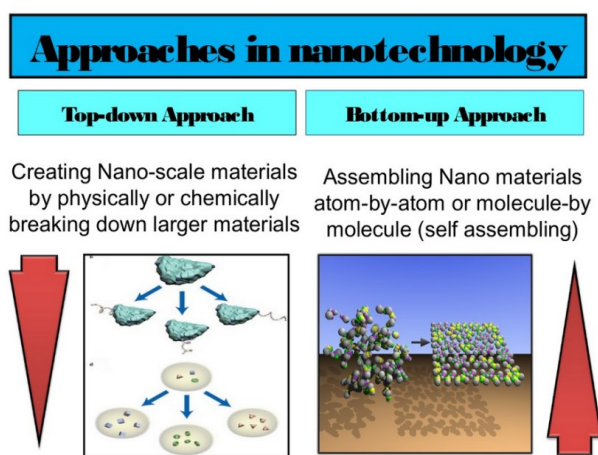
Fig. 1-5: Top-down and bottom-up approach of nanotechnology.[14b]

In the synthesis of two-dimensional coordination compounds, a bottom-up method can be considered more advantageous over the top-down method. For example, increased flexibility over their compositions and structures can be obtained as they are not fixed by the bulk materials. On the contrary, the bottom-up approach allows almost any plausible two-dimensional compounds to be designed and synthesized accordingly. Furthermore, a whole new range of 2D materials could be tailor-made according to their required properties, starting from the zero or one dimensional building blocks. Such a strategy precludes the dependence on the structure of 3D bulk materials and enables the customizability of the resulting 2D compounds, by simply changing the metal node, or modifying the shape and coordination geometry of the organic linker. As such, the diversity and utility of nanosheets can be greatly broadened.

1.4.   Potential of 2D Coordination Nanosheets

Kambe *et al.* have previously described the synthesis of a π-conjugated bis(dithiolato)nickel nanosheet (**NiDT**) *via* a bottom-up approach. [16] This two-dimensional coordination nanosheet coined CONASH was formed from the reaction between benzenehexathiol (BHT) and nickel(II) acetate in a biphasic mixture of water and dichloromethane. With benzenehexathiol acting as a tri-chelating ligand to extend outwards from the vertices of the ligand resembling an equilateral triangle and the nickel(II) ions in a square planer coordination mode, a two-dimensional planar **NiDT** nanosheet was formed from the bottom-up method.

The **NiDT** product was formed at the interface of the immiscible reagent solutions of dichloromethane and aqueous solutions. This protocol of utilizing the interfacial layer of two immiscible liquids for the synthesis and growth of a 2D material is highly effective because the two-dimensional interface encourages the arrangement of the metal ions and ligands in a planar formation and aids the formation of a planar compound. Alternatively, vigorous mixing of the solution mixture or employing a liquid-liquid layering technique containing both starting materials dissolved in miscible mutually miscible solvents to synthesize **NiDT** would result in precipitation of amorphous solids rather than forming 2D sheets. A slightly modified method was used to form the thinner layers of **NiDT**. Instead of a liquid-liquid interfacial reaction, a gas-liquid interfacial reaction with calculated amounts of the ligand was added to the surface of the aqueous metal ion solution for the formation of the compound on the aqueous solution surface.

Furthermore, similar to the characteristics of metalladithiolene complexes, redox control of **NiDT** has been proved to be possible. The nanosheet, as prepared with a thickness of 1-2 μm, was found to have an average oxidation state of -3/4. The as-prepared **NiDT** (ap-1) could be fully oxidized to 0 (ox-1) or fully reduced to -1 (red-1) using tris(4-bromophenyl)ammoniumyl hexachloroantimonate and sodium tetracyanoquinodimethane respectively (Fig. 1-6).[17] Fully oxidized **NiDT** exhibited very high conductivity for a coordination compound with 1.6×10^2 S cm^{-1} at 300 K.
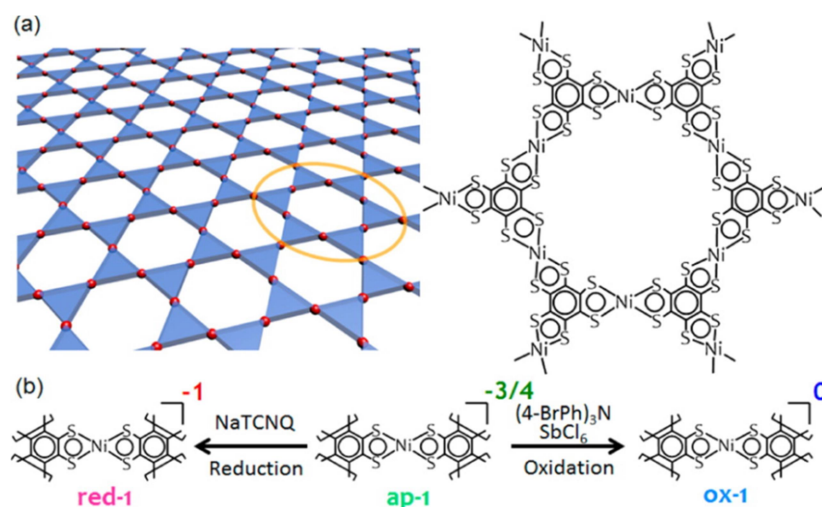
Fig. 1-6: (a) Chemical structure of the bis(dithiolato)nickel **NiDT** nanosheet. (b) Schematic illustration on redox control in the stacked nanosheet. Reprinted with permission from ref. 17. Copyright (2014) American Chemical Society.

Other than its interesting chemistry and conductivity, this particular nanosheet has also been predicted to be an organic topological insulator by Wang *et al.*[18] A topological insulator is defined by the existence of a robust conducting edge or surface states on the boundary of normal insulators. This essentially means that a single layer of the bis(dithiolato)nickel nanosheet is predicted to be an insulator with some exotic metallic states at the edges of the sheet (Fig. 1-7). These states have a topological origin, which makes the electrons travelling on such surfaces insensitive to scattering by impurities. As such, they have promising potential in technological applications in spintronic and quantum computation devices.[19]

Recently, a slightly modified ligand from BHT has also been used to synthesize 2D sheets. Sun *et al.* has discussed in two separate papers on the formation of two different types of CONASHs from the 1,3,5-triaminobenzene-2,4,6-trithiol ligand.[20] The bis(aminothiolato)nickel (**NiAT**) formed could be interconverted reversibly to form bis(iminothiolato)nickel (**NiIT**), but both compounds have a distinct 5 orders difference in their electrical conductivity, from 3×10^{-6} S cm^{-1} to 1×10^{-1} S cm^{-1}.
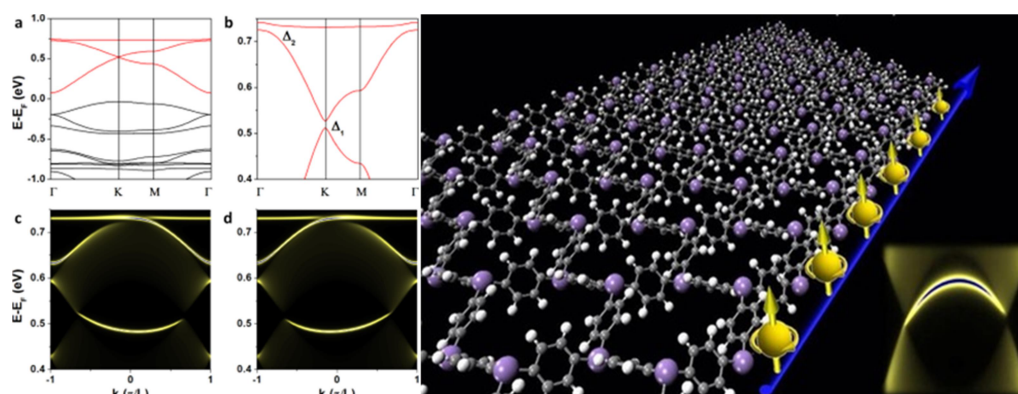
Fig. 1-7: Bis(dithiolato)nickel complex nanosheet predicted to be a topological insulator (left), which has conducting electrons at its edge (as illustrated, right). Reprinted with permission from ref. 18. Copyright (2013) American Chemical Society.

With such possibilities obtainable from just one type of nanosheet, two-dimensional coordination compounds made from the bottom-up approach shows great potential for applications in many areas. Since the bottom-up method allows the composition, structure and various properties to be tailored at will, the new or improved properties which are achievable from new compounds stimulates the great interest and excitement in this area of research.

1.5. The Choice of Ligand
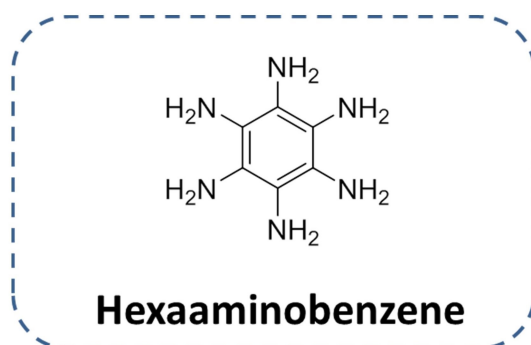
In this research, hexaaminobenzene (**HAB**) was chosen as the ligand used for the synthesis of the sheets. Noro *et al.* have previously reported their success in fabricating metal-organic thin-film transistors by using semiconducting bis(*o*-diiminobenzosemiquinonato)nickel(II) complexes and their derivatives, which have successfully shown ambipolar characteristics (Fig. 1-8).[21] Such ambipolar properties were also observed when aromatic amines are used.
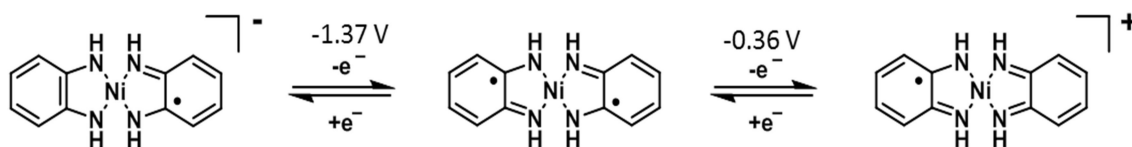

Fig. 1-8: Ambipolar properties of aromatic amines coordinated to nickel(II) ions. $E_{1/2}$ values versus ferrocenium/ferrocene couple.

Although it is unclear if ambipolar characteristics would be observed in nanosheets containing such moieties, the lack of study in utilizing such motifs provides an opportunity to investigate the use of related highly symmetrical and multi-dentate aromatic amines that are coordinated to Ni(II) ions, to form such 2D materials.

A similar two-dimensional system of nickel(II) ions coordinated with aromatic amines of $Ni_3(2,3,6,7,10,11\text{-hexaiminotriphenylene})_2$ was recently reported by Sheberla *et al.*[22] In their report, the hexaaminotriphenylene ligand coordinated to nickel(II) ions forms slipped-stacked layered structure with an interlayer distance of 3.3 Å. This material displayed high electrical conductivity of up to 40 S·cm^{-1} at room temperature

(Fig. 1-9), and such a system is similar to the one that was previously studied in our group.
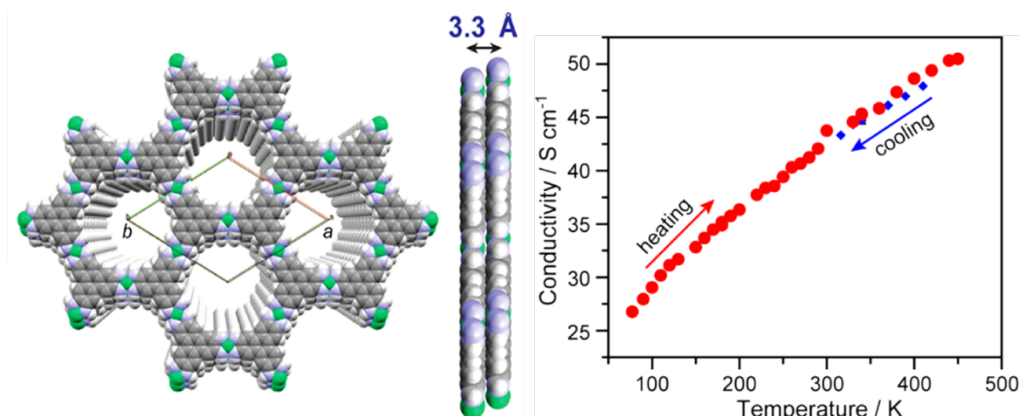
Fig. 1-9: Ni_3(2,3,6,7,10,11-hexaiminotriphenylene)$_2$ reported by Sheberla et al. which shows high electrical conductivity. Reprinted with permission from ref. 22. Copyright (2014) American Chemical Society.

1.6.   Aim of Research

As an extension and continuation of the research program in the Nishihara group, the use of the hexaaminobenzene ligand to create 2D nanosheets was investigated, and its synthesis and physicochemical properties will be thoroughly discussed in later chapters of this dissertation. Similar to the benzenehexathiol ligand, the hexaaminobenzene ligand is also a multi-chelating ligand which can extend in three directions when coordinated with any square planar type of metal ions. As such, it is plausible that a two-dimensional planar nanosheet with a C_6 symmetry axis can be achieved based on the selective design strategy involving a nickel bis(diimino) moiety. It is also reasonable to expect that the desired product would be isostructural to the **NiDT** nanosheet. In addition, it is also proposed that this system would contain stronger interaction between the nickel ion and the ligand, since the hexaaminobenzene is smaller than that of the hexaaminotriphenylene ligand.

The following chapter of this thesis focuses on the screening and optimization reactions, for the synthesis of various hexaaminobenzene-based nickel(II) nanosheets, including the synthesis of the ligand, nanosheets, and the analysis of their structure and the physicochemical properties. The use of a new electrochemical method to synthesize the hexaaminobenzene-based nickel(II) nanosheets would be covered in Chapter 3. The investigation of related systems containing other metal ions such as palladium(II) and platinum(II) and their corresponding properties, will be discussed in the penultimate chapter of this dissertation. Last but not least, the future work and further prospects of this research work covered in the last chapter.

1.7.   References

1.   X. Chen, B. Ye, M. Tong, *Coord. Chem. Rev.,* **2005**, *249*, 545-65.

2.   A. R. Millward, O. M. Yaghi, *J. Am. Chem. Soc.*, **2005**, *127*, 17998-9.

3.   (a) C. Y. Su, Y. P. Cai, C. L. Chen, M. D. Smith, W. Kaim, H. C. Z. Loye, *J. Am. Chem. Soc.*, **2003**, *125*, 8595-613.

(b) Y. Feng, D.-B. Wang, B. Wan, X.-H. Li, Q. Shi, *Inorg. Chim. Acta.,* **2014**, *413*, 187-93.

4.   (a) B. Chen, S. Xiang, G. Qian, *Acc. Chem. Res.,* **2010**, *43*, 1115-24.

(b) A. Phan, C. J. Doonan, F. J. Uribe-Romo, C. Knobler, M. O'Keeffe, O. M. Yaghi, *Acc. Chem. Res.*, **2010**, *43*, 58-67.

(c) G. Ferey, *Chem. Soc. Rev.*, **2008**, *37*, 191-214.

(d) M. D. Allendorf, C. A. Bauer, R. K. Bhakta, R. J. Houk, *Chem. Soc. Rev.*, **2009**, *38*, 1330-52.

(e) I. Imaz, M. Rubio-Martinez, J. An, I. Sole-Font, N. L. Rosi, D. Maspoch, *Chem. Commun.*, **2011**, *47*, 7287-302.

(f) Y. Cui, Y. Yue, G. Qian, B. Chen, *Chem. Rev.*, **2012**, *112*, 1126-62.

5.   D. R. Dreyer, R. S. Ruoff , C. W. Bielawski, *Angew. Chem. Int. Ed.,* **2010**, *49*, 9336-44.

6.   (a) M. C. Tringides, M. Jałochowski, E. Bauer, *Physics Today*, **2007**, *60*, 50.

(b) V. K. Arora, *J. Vac. Sci. Technol.,* **1982**, *20*, 94.

(c) Kathleenlanz. "Graphene Presentation" Web.

< https://www.emaze.com/@ACCCFZLC/Graphene-Presntation>

7.   (a) M. Osada, T. Sasaki, *J. Mater. Chem.,* **2009**, *19*, 2503-11.

(b) C. Wang, Y. Zhou, M. Ge, X. Xu, Z. Zhang, J. Z. Jiang, *J. Am. Chem. Soc.,* **2009**, *132*, 46-7.

(c) T. Yu, B. Lim, Y. Xia, *Angew. Chem. Int. Ed.,* **2010**, *122*, 4586-9; *Angew. Chem. Int. Ed.,* **2010**, *49*, 4484-7.

(d) W. Choi, I. Lahiri, R. Seelaboyina, Y. S. Kang, *Crit. Rev. Solid State Mater. Sci.,* **2010**, *35*, 52-71.

8.   (a) L. Dong, R. R. S. Gari, Z. Li, M. M. Craig, S. Hou, *Carbon*, **2010**, *48*, 781.

(b) X. Y. Qi, H. Li, J. W. Y. Lam, X. T. Yuan, J. Wei, B. Z. Tang and H. Zhang, *Adv. Mater.*, **2012**, *24*, 4191.

(c) Z. J. Wang, J. Zhang, P. Chen, X. Z. Zhou, Y. L. Yang, S. X. Wu, L. Niu, Y. Han, L. H. Wang, P. Chen, F. Boey, Q. C. Zhang, B. Liedberg,H. Zhang, *Biosens. Bioelectron.*, **2011**, *26*, 3881.

9.   (a) J. Mei, T. Liao, L. Kou, Z. Sun, *Adv. Mater.*, **2017**, 1700176.

(b) X. Wang, Q. Weng, Y. Yang, Y. Bando, D. Golberg, *Chem. Soc. Rev.,* **2016**, *45*, 4042-4073.

10.   N. S. Hush, *Coord. Chem. Rev.,* **1985**, *64*, 135-157.

11.   X. Qi, C. Tan, J. Wei, H. Zhang, *Nanoscale*, 2013, **5**, 1440-51.

12.   W. Jie, J. Hao, *Nanoscale*, **2014**, *6*, 6346–6362.

13.   (a) H. S. Lee, S.-W. Min, M. K. Park, Y. T. Lee, P. J. Jeon, J. H. Kim, S. Ryu, S. Im, *Small,* **2012**, *8*, 3111-5.

(b) Z. Zeng, Z. Yin, X. Huang, H. Li, Q. He, G. Lu, F. Boey, H. Zhang, *Angew. Chem. Int. Ed.,* **2011**, *50*, 11093-7.

(c) D. Yan, J. Lu, M. Wei, J. Han, J. Ma, F. Li, D. G. Evans, X. Duan, *Angew. Chem. Int. Ed.,* **2009**, *48*, 3073-6.

14.   (a) "Exfoliation and Lithography." *Graphene Laboratory*. Group for Physics of Ordered Nanostructures and New Materials in Photonics. Web. <http://www.graphene.ac.rs/exfoliation.html>.

(b) Sujani, Sathya. "Approaches in Nanotechnology." *Nanotechnology: Basic Introduction to the Nanotechnology.* Web. <http://www.slideshare.net/sasujani/nanotechnology-basic-introduction-to-the-nanotechnology>.

15.   P. Iqbal, J. A. Preece, P. M. Mendes, Nanotechnology: The "Top-Down" and "Bottom-Up" Approaches. Supramolecular Chemistry: From Molecules to Nanomaterials, 2012.

16.   T. Kambe, R. Sakamoto, K. Hoshiko, K. Takada, M. Miyachi, J.-H. Ryu, S. Sasaki, J. Kim, K. Nakazato, M. Takata, H. Nishihara, *J. Am. Chem. Soc.*, **2013**, *135*, 2462-5.

17.   T. Kambe, R. Sakamoto, T. Kusamoto, T. Pal, N. Fukui, T. Shimojima, Z. Wang, T. Hirahara, K. Ishizaka, S. Hasegawa, F. Liu, H. Nishihara, *J. Am. Chem. Soc.*, **2014**, *136*, 14357-60.

18.   *Z. F. Wang, N. Su, F. Liu, *Nano Lett.,* **2013**, *13*, 2842-5.*

19. Y. Xu, I. Miotkowski, C. Liu, J. Tian, H. Nam, N. Alidoust, J. Hu, C.-K. Shih, M. Z. Hasan, Y. P. Chen, *Nat. Phys.,* **2014***, 10*, 956–63.

20. (a) X. Sun, K.-H. Wu, R. Sakamoto, T. Kusamoto, H. Maeda, H. Nishihara, *Chem. Lett.,* **2017**, *46*, 8, 1072.
    (b) X. Sun, K.-H. Wu, R. Sakamoto, T. Kusamoto, H. Maeda, X. Ni, W. Jiang, F. Liu, S. Sasaki, H. Masunaga, H. Nishihara, *Chem. Sci.,* **2017**, *8*, 8078.

21. (a) S. Noro, T. Takenobu, Y. Iwasa, H.-C. Chang, S. Kitagawa, T. Akutagawa, T. Nakamura, *Adv. Mater.,* **2008**, *20*, 3399-403.
    (b) S. Noro, H.-C. Chang, T. Takenobu, Y. Murayama, T. Kanbara, T. Aoyama, T. Sassa, T. Wada, D. Tanaka, S. Kitagawa, Y. Iwasa, T. Akutagawa, T. Nakamura, *J. Am. Chem. Soc.,* **2005**, *127*, 10012-3.

22. D. Sheberla, L. Sun, M. A. Blood-Forsythe, S. Er, C. R. Wade, C. K. Brozek, A. Aspuru-Guzik, M. Dincă, *J. Am. Chem. Soc.,* **2014***, 136,* 8859-8862.

Chapter 2

CHEMICAL BIS(DIIMINO)NICKEL(II) NANOSHEETS

## 2   CHEMICAL BIS(DIIMINO)NICKEL(II) NANOSHEETS

2.1.   Introduction

As discussed in the introductory chapter, the hexaaminobenzene (**HAB**) ligand is isostructural to the benzahexathiol ligand, which is one of the reasons why the ligand was chosen. As such, when the research of bis(diimino)nickel(II) nanosheets (**NiDI**) made from the hexaaminobenzene first started, a similar synthetic method to the **NiDT** which was also synthesized in Nishihara laboratory was attempted.[1]

For **NiDT**, a liquid-liquid interfacial system was used for its bulk synthesis. The **NiDT** was formed at the interface of the immiscible reagent solutions of benzahexathiol in dichloromethane and aqueous solution of nickel(II) ions. For the thinner layers of **NiDT**, instead of a liquid-liquid interfacial reaction, a gas-liquid interfacial reaction with controlled amounts of the ligand dissolved in organic solvent was added to the surface of the aqueous metal ion solution for the formation of the compound on the aqueous solution surface.

When the system is adapted for **NiDI**, as the **HAB** ligand is used in its trihydrochloride form (**HAB**·3HCl), **HAB** was used in an aqueous solution instead, and the nickel(II) ions were dissolved in an organic phase. The aim was to let the reaction happen at the interface of the immiscible ether and water solutions. As illustrated in Fig. 2-1, 10 mL of bis(diacetylacetonato)nickel(II) in ether was layered onto an aqueous solution of 5 mL aqueous ammonia mixed with 10 mL of **HAB**·3HCl. However, as seen in the figure, the resulting **NiDI** sample is not cleanly formed between the two immiscible solutions unlike that in **NiDT**. Instead, the formation of the compound could be found both at the interface and along the vial walls. A lot of amorphous solids could also be seen in the system.

In addition, when a similar set up was carried out in the glovebox under argon atmosphere, it was found that the reaction did not take place and after a very long time, a small amount of brown solids could be seen at the interface (Fig. 2-2). It could be
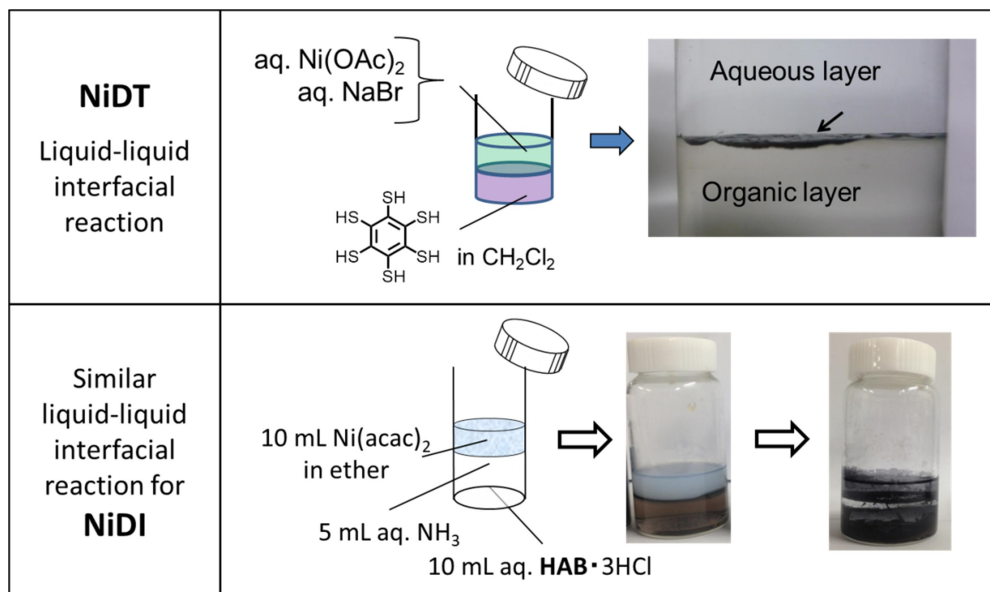
Fig. 2-1: Liquid-liquid interfacial syntheses of **NiDT** as compared to **NiDI**.
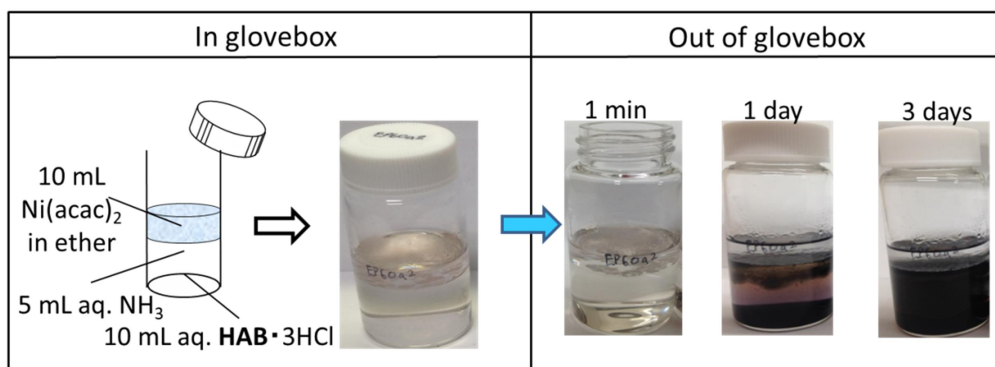
Fig. 2-2: Liquid-liquid interfacial synthesis of **NiDI** set up in the glovebox, which was then taken out.

observed that there is a difference in the visual properties of the nanosheets formed in and out of the glove box. As seen in Fig. 2-1, the resulting sample that was formed under atmospheric conditions is black and sinks to the bottom of the reaction vial. On the other hand, the **NiDI** which was synthesized in the glove box, was visibly determined to be light brown and remained at the interface of the two liquids. These two results are very different, which led to the hypothesis that oxygen could play a part in the formation of **NiDI**.

To confirm the hypothesis, the system that was set up and left to stand for many days in the glove box, was taken out of the glove box and then observed. Fig. 2-2 shows

what happened to the reaction system after 1 minute, 1 day and 3 days. It can be seen that after 1 minute (almost immediately), the nanosheets formed at the interface of the liquids turned darker. The vial was then capped and left to stand, and the whole system could be seen to turn visibly much darker and the system very much resembled that of the system that was made outside the glovebox. On the other hand, the control which was left in the glove box did not have such drastic colour changes. The observations suggest that oxygen is required for the formation of **NiDI**. These investigations then paved the way for the current research thesis and would be described in the next sections.

2.2.   Optimizing the NiDI system

From the previous section, two important findings of the **NiDI** system have been established. Firstly, oxidation is required for the formation of **NiDI**. This can be seen from the fact that the reaction does not occur when the system is set up in the glove box but occurs rapidly when the reaction vial is exposed to atmospheric air. Secondly, it can be observed that there is a need to optimize or develop a new system for the formation of the **NiDI** system since the tried and tested liquid-liquid interfacial methods of other systems do not work well.

Keeping in mind the two findings, the journey to find the best method for the synthesis of **NiDI** began. Firstly, why the current results are obtained should be explained. The interface of the two liquids should be the only place where all the reagents required for the formation are present, so theoretically that should be the only place where the final product is formed, which is like how usual liquid-liquid interfacial reactions are carried out. Referring to Fig. 2-3, in the case of **NiDI**, things start getting complicated since the oxygen from the atmospheric air is also involved in the reaction. The oxygen comes from the top of the system, so the reaction occurs at other parts of the reaction vial other than just the interface of the two liquids.

Usual liquid-liquid interfacial reactions	Liquid-liquid interfacial reaction for **NiDI**	New homogeneous system
	O_2	O_2
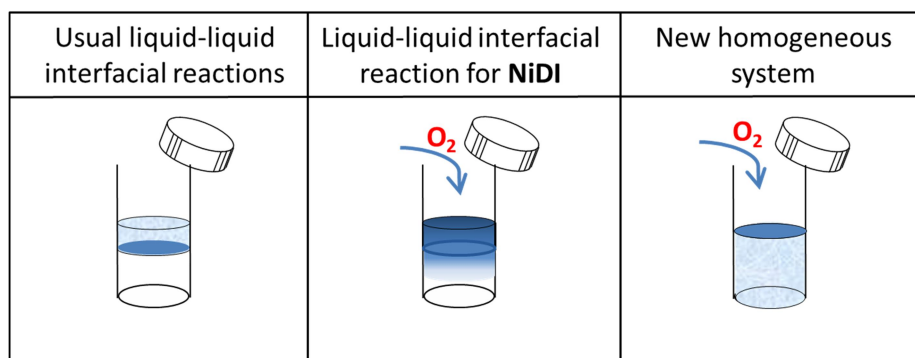
Fig. 2-3: Illustration showing the difference in the usual liquid-liquid interfacial system as compared to the **NiDI** case, as well as the postulated new homogenous system.

As this **NiDI** system is characteristically different from the other systems, a method to make use of the oxygen coming from the top of the system to form some

films should be developed. This meant that the interface where the reaction is happening should be at the top. The interface is important for the formation of good two-dimensional films. As such, the idea of having a homogenous system with all the reagents inside was conceived, and that the oxygen which comes from the top would be the determining factor for formation of **NiDI** on the homogeneous solution interface. As illustrated in Fig. 2-3, it is postulated that a target film would be formed at the top of the homogeneous system when oxygen is also considered as one of the variables.

Since **HAB**·3HCl easily solubilizes in water, the homogeneous system should be an aqueous system, and a new nickel(II) ion source should be used. As such, nickel(II) acetate was used as the nickel(II) ion source. Also, it is important that the new homogeneous system has to be set up in the glove box, then taken out and left undisturbed in atmospheric conditions, as amorphous solids would be easily formed if the solution is quickly mixed with oxygen.

2.3.   Chemical Synthesis of NiDI

The optimized synthesis of the **NIDI** nanosheet formation is performed through an oxidation assisted reaction and is formed by the reaction between the hexaaminobenzene trihydrochloride ligand (0.4 mM) and nickel(II) acetate (15 mM) in 4.5 M excess concentrated ammonia solution. By varying the rate and amount of dioxygen introduced into the gas phase just above the aqueous solution of reaction, different thickness of crystalline black sheets were formed at the surface of the solution, affording the **NiDI** nanosheet as shown in Fig. 2-4. Fig. 2-5(a) - (h) shows the formation of the **NiDI** nanosheet at different time intervals after the setting up of the experiment. The metallic lustre of thicker nanosheets can be observed in Fig. 2-4, indicating a certain level of crystallinity of the **NiDI** CONASH.
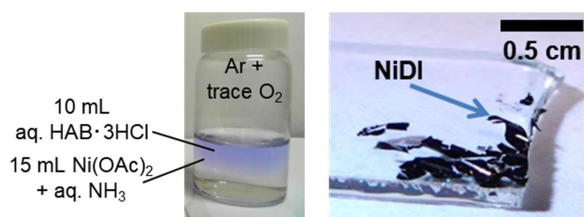

Fig. 2-4: Reaction conditions (left) and crystalline **NiDI** which has been transferred onto a glass substrate (right).
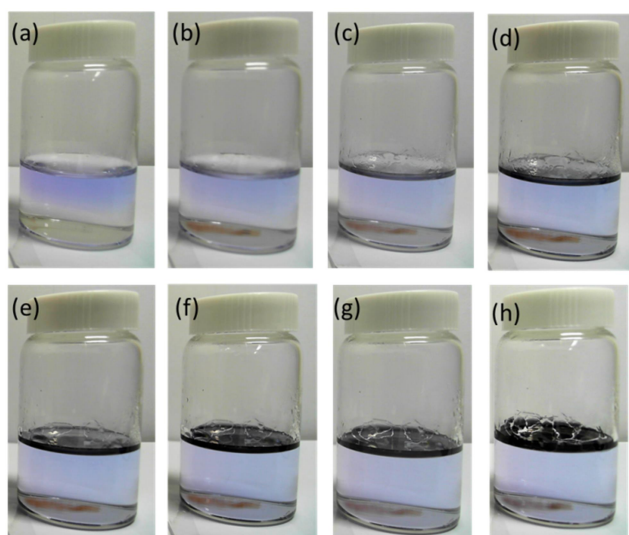
Fig. 2-5: Photographs taken during the formation of chemically synthesized **NiDI**. (a) Beginning of experiment (0 hours). (b) After 7 hours. (c) After 15 hours. (d) After 20 hours. (e) After 1 day (26 hours). (f) After 1.5 days (approximately 36 hours). (g) After 2 days (approximately 48 hours). (h) After 3 days (approximately 72 hours).

This novel sheet is slowly formed on the calm liquid surface over time, as oxygen is required for the formation. This is due to the need for the biradical formation with structures similar to bis(*o*-diiminobenzosemiquinonato)nickel(II), Ni(isq)$_2$ (isq = *o*-diiminobenzosemiquinonate), which has been synthesized under air. The slow exposure to atmospheric oxygen is the crux for the high crystallinity of the sheets formed. With this gas/liquid interfacial reaction method based on the previous interfacial synthesis, we are able to obtain large centimetre-scale **NiDI** nanosheets with high crystallinity visible to the naked eye as shown in Fig. 2-4.

The formation mechanism is shown in Fig. 2-6. In the as-prepared solution, two hexaaminobenzene ligands, which are formed by the neutralization of the trihydrochloride salts with ammonia, reversibly coordinate with the nickel ion since the coordination ability of anilines is not strong enough. As dioxygen is introduced, a pair of the coordinated amines of each ligand is oxidized, resulting in a π-conjugated five membered metallacycle, which dramatically improves the coordination ability of the ligand and stabilizes the complex. Then, the other two pairs of free amines on the ligand are also oxidized to coordinate stably to other nickel ions, which then coordinate with other ligands. Eventually, the complexes expand to become a large coordinated sheet on the gas/liquid interface.
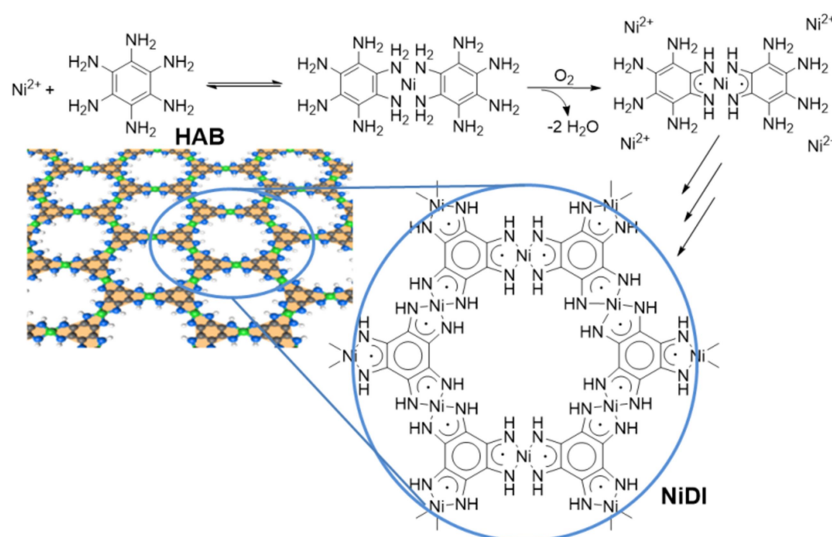
Fig. 2-6: Mechanism of **NiDI** formation and the resulting kagome lattice.

2.4. Characterization and Structure

2.4.1. X-ray photoelectron spectroscopy (XPS)
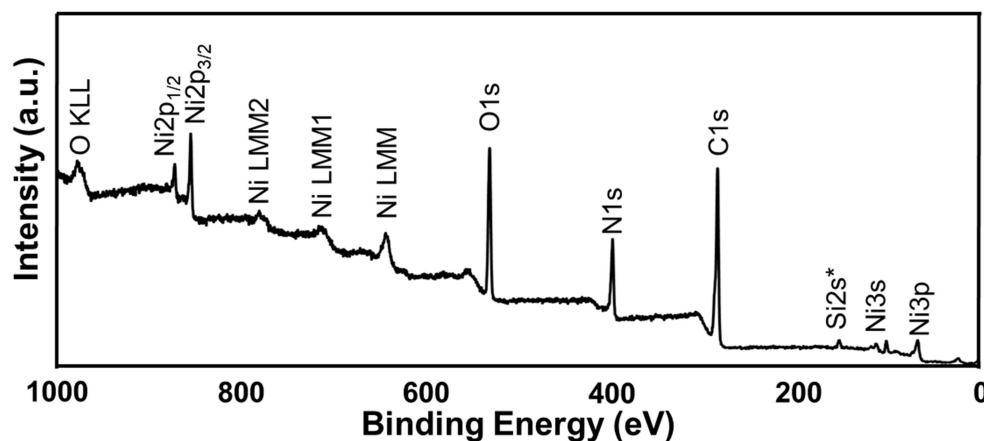
Fig. 2-7: XPS spectrum of neutral **NiDI** films formed by the chemical method. The sample was measured on a silicon substrate which explains the presence of Si2s peaks present in the spectrum.

Characterizing the **NiDI** sheets using X-ray photoelectron spectroscopy (XPS) showed the presence of N1s, Ni2p, and C1s peaks, proving the formation of the **NiDI** nanosheet. The Si2s peak is from the SiO_2 substrate on which the **NiDI** was transferred to. The elemental ratio of nickel to nitrogen was found to be 1:4.2, which is close to the expected 1:4 ratio for the **NiDI** nanosheet.

From the XPS spectrum, the **NiDI** CONASH formed is found to be neutral, with the basic structure of $[\textbf{NiDI}]^0$ similar to the centre neutral complex in Fig. 1-8. Other than the presence of the peaks which represents the presence of **NiDI**, substrate peaks and O1s peaks which are from ubiquitous oxygen or small amount of water molecules adsorbed onto the films, no other peaks are present. For example, Cl peaks, originating from the **HAB**·3HCl ligand, are absent. This shows the absence of any trapped anionic chlorides to compensate a possible cationic structure.

In addition, when the high-resolution XPS analyses of the Ni2p and N1s regions are observed, a single type of Ni and N environment is seen (*c.f.* Fig. 3-4). This suggests that possible cations, such as extraneous Ni^{2+} or NH_4^+ ions, to balance anionic **NiDI** is

absent. Since no other cations or anions could be formed from the reagents used, it can be inferred that a neutral form of **NiDI** has been obtained.

2.4.2. *Infrared spectroscopy*

Infrared spectroscopy of pelletized **NiDI** ground with solid KBr gave distinct bands which correspond to the expected structure of the **NiDI** and are in similar to those observed for mononuclear equivalent bis(*o*-diiminobenzosemiquinonato)nickel(II), Ni(isq)$_2$ (isq = *o*-diiminobenzosemiquinonate). The representative peaks are however much broader than the peaks of Ni(isq)$_2$ because of the polymeric structure and presence of hydrogen bonding in **NiDI**. This causes the many similar bonds present to exhibit slightly different environments from their counterparts and lead to a broadening of the peaks found at their expected wavenumber range. Fig. 2-8 shows the IR spectra of **NiDI** and mononuclear bis(o-diiminobenzosemiquinonate) nickel(II) complex.
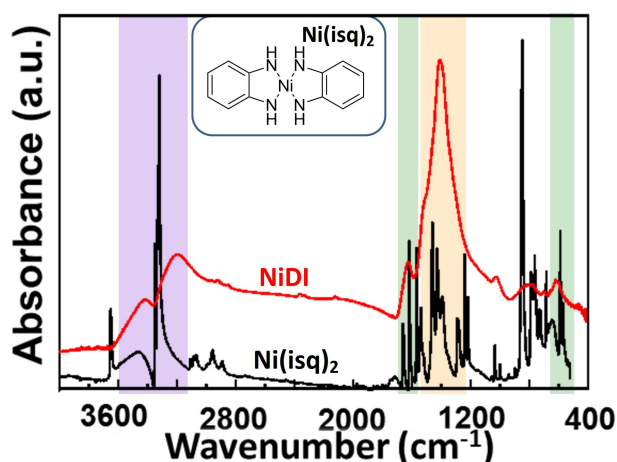

Fig. 2-8: IR spectra of **NiDI** (red) and mononuclear bis(*o*-diiminobenzosemiquinonate) nickel(II) complex (black). The coloured regions are the peaks assigned to N-H stretching (purple), aromatic ring (green) and C=N stretching (orange) respectively. Inset shows the structure of the mononuclear Ni(isq)$_2$ complex.

The bands at about 3200 cm^{-1} and 3440 cm^{-1} can be assigned to the N-H stretching (purple) while peaks at 640 cm^{-1} and 1600 cm^{-1} can be assigned to be the aromatic ring (green) while the strong signal at about 1400 cm^{-1} matches with C=N stretching (orange). Based on these assignments, it can be inferred that the structure of the **NiDI** nanosheet most likely to be that of the proposed structure in Fig 2-6.

2.4.3. *Powder X-ray diffraction*

Powder X-ray diffraction (PXRD) data obtained for the bulk **NiDI** sheet obtained using high energy synchrotron radiation (λ = 0.80 Å) showed distinct peaks, further proving the crystallinity of the product formed. Further analysis of the pattern, as shown in Fig. 2-9, were found to match the pattern obtained from simulated data of an eclipsed nanosheet array with the crystal lattice parameters of $a = b$ = 13.01 Å and c = 3.25 Å. These values were also found to match the ones obtained from DFT calculations which were based on an extended **NiDI** lattice.
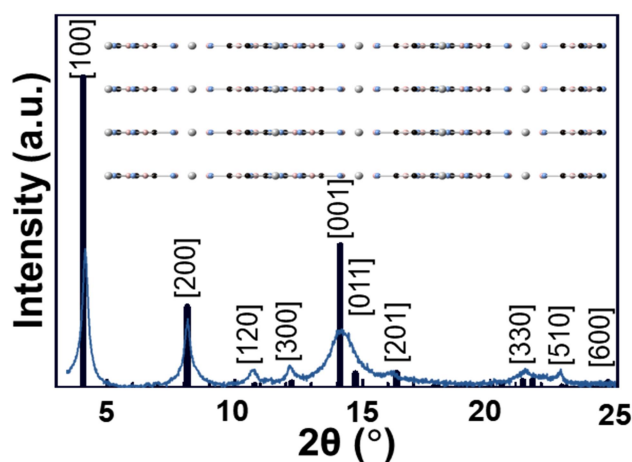
Fig. 2-9: Powder XRD spectrum of experimental **NiDI** (blue) matching with simulated spectrum of eclipsed **NiDI**. Inset shows the illustration of eclipsed **NiDI**.

The two relatively sharp peaks at 2θ = 4.05° and 8.05° belong to the [100] and [200] diffraction planes, while the relatively broad peak at 2θ = 14.10° was found to be a combined signal from the [001] and [011] planes. This is most likely due to the slightly poorer long-range order in the stacking of the sheets in the crystallographic c-axis. The remaining peaks have been assigned to the [120], [300], [201], [330], [510] and [600] planes accordingly.

The simulated pattern of the **NiDI** sheet stacked in a staggered pattern was also calculated and compared but is found to be less well-matched as compared to the eclipsed form as shown in Fig. 2-10.
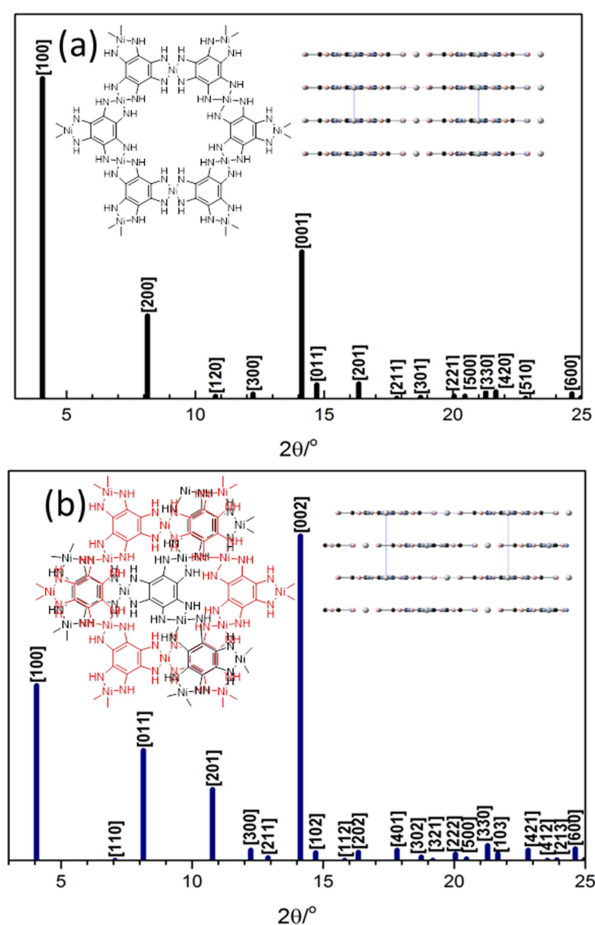
Fig. 2-10: (a) Simulated pXRD spectra and structure of eclipsed **NiDI** nanosheet.
(b) Simulated pXRD spectra and structure of staggered **NiDI** nanosheet
(wavelength = 0.80 Å).

2.4.4. *Microscopy images*

The **NiDI** sample was determined to have a sheet-like layered structure under the different microscopes. When transferred onto substrates and then observed under the optical microscope, large domains greater than a few hundreds of micrometres can be observed (see Fig. 2-11(a)). This further supports the large centimetre-size black film as seen in Fig. 2-4, and this film is also clearly a continuous sheet with rather large domains as observed by microscopy.

The sheet-like layered topology can also be seen clearly from the scanning electron microscopy (SEM) and transmission electron microscopy (TEM) images in Fig. 2-11(b) and (c). Atomic force microscopy (AFM) images of the control **NiDI** sample
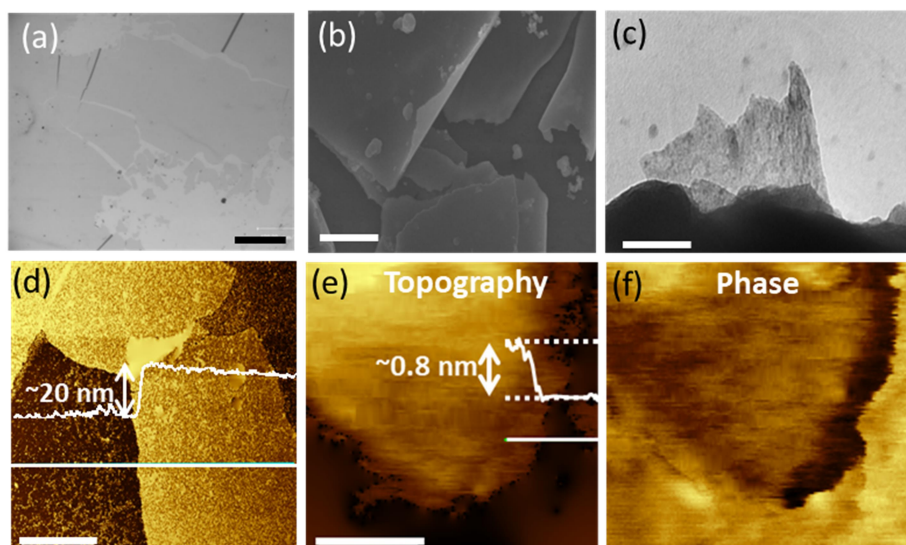
Fig. 2-11: Microscopy images of **NiDI** sheet. (a) Optical microscopy image. Scale bar represents 100 μm. (b) SEM image. Scale bar represents 5 μm. (c) TEM image. Scale bar represents 100 nm. (d) AFM image and height profile of large domain **NiDI**. Scale bar represents 5 μm. (e) Topography AFM image and height profile of thin **NiDI** at edges. Scale bar represents 50 nm. (f) Phase diagram of (e).

(see Fig. 2-11(d)), revealed that the sheet thickness is approximately 20 nm and spans an area of approximately 10 μm by 20 μm.

Further control of the exposure time to dioxygen resulted in the detection of even thinner sheets with an edge of just 0.8 nm thickness, corresponding to a single layer nanosheet, as seen in Fig. 2-11(e). To confirm that this is indeed a monolayer **NiDI** and not just simply a step edge of the substrate, the corresponding phase diagram is given in Fig. 2-11(f). This shows that the area of monolayer mentioned is a totally different phase from the surroundings, indicating that it is a monolayer directly on the SiO_2 substrate.

2.5. Physical Properties

2.5.1. Cyclic Voltammetry

The redox activity of a **NiDI** nanosheet deposited on HOPG was investigated using cyclic voltammetry (CV) in 1 M Bu$_4$NClO$_4$-MeCN. The redox behaviour of the **NiDI** nanosheet shown in the steady state CV in Fig. 2-12 is not very reversible unlike the mononuclear complexes of bis(diimino)nickel derivatives[2]; however, oxidation and rereduction peaks appear at approximately 0.28 V vs. ferrocenium/ferrocene (Fc$^+$/Fc), indicating the redox reaction is chemically reversible. This peak couple can be ascribed to [**NiDI**]$^+$/[**NiDI**]^0 based on the redox behaviour of the mononuclear bis(diimino)nickel complex.
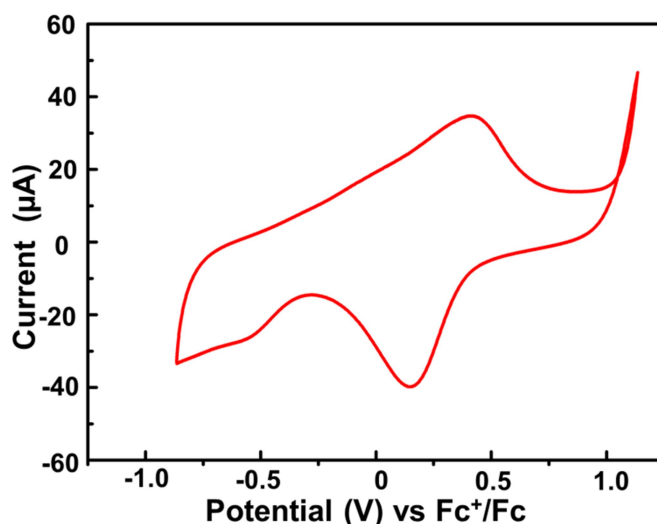
Fig. 2-12: Cyclic voltammogram of chemically synthesized **NiDI** nanosheet on HOPG vs Fc$^+$/Fc.

2.5.2. Conductivity

Electrical conductivity of a **NiDI** nanosheet in its pelletized form was measured using a four-terminal method under helium while varying the temperature. Fig. 2-13 shows the temperature dependent electrical resistivity of **NiDI** which rises as a function of inverse temperature. The electrical conductivity (σ) of the **NiDI** nanosheet increased

with temperature and was 1.3×10^{-3} S·cm^{-1} at 298 K, indicating its semiconducting nature with the activation energy of 0.16 eV. Similar results of two independent samples indicating the repeatability of the measurement is given in Fig. 2-14. The activation energy was calculated as follows: Gradient of Ln(Resistivity) graphs = $E_a/1000k_B$; E_{a1} = 0.163 eV; E_{a2} = 0.160 eV (see appendix 1).
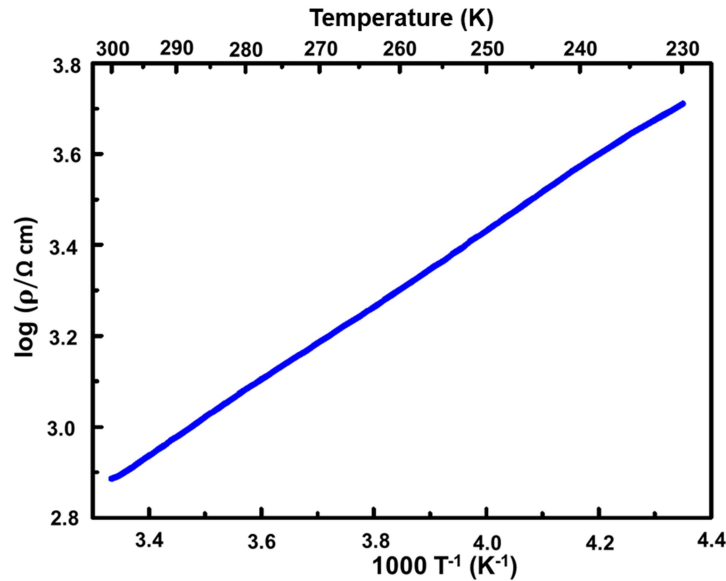

Fig. 2-13: Temperature-dependent resistivity of **NiDI** CONASH plotted as log(ρ) vs. $1000T^{-1}$.
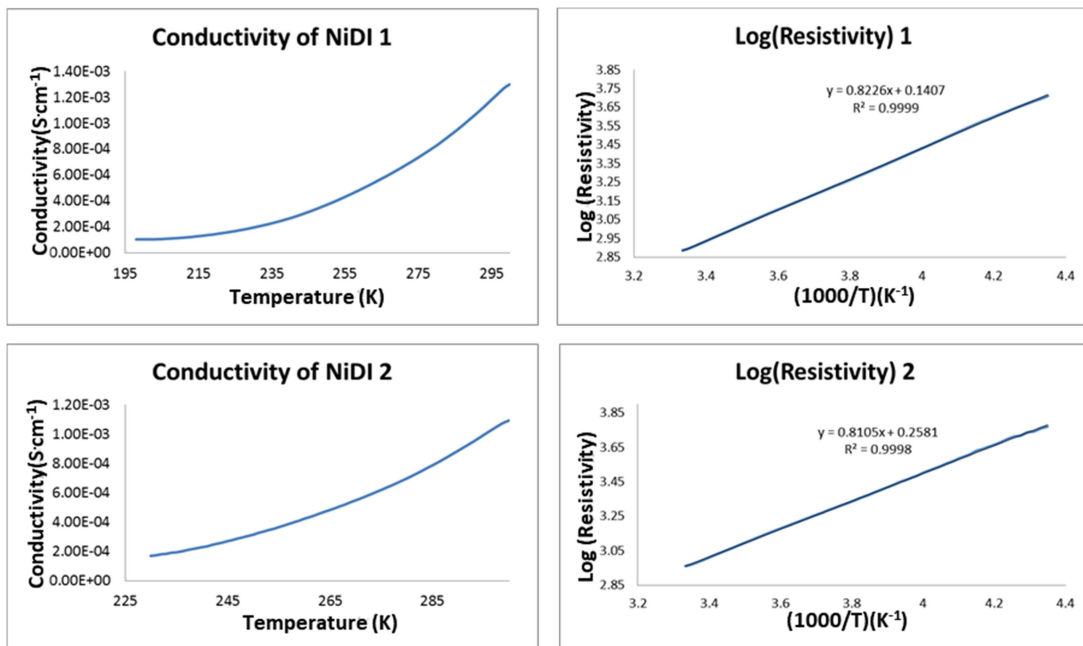
Fig. 2-14: Temperature-dependent resistivity of 2 independent **NiDI** CONASH plotted as conductivity vs. temperature and log(ρ) vs. $1000T^{-1}$.

While the σ value obtained is lower than the ones obtained from the pelletized sample of structurally similar **NiDT** nanosheet (0.15 S·cm^{-1})[1b] or Ni$_3$(HITP)$_2$ nanosheet (2 S·cm^{-1})[3], they were still comparable to other films formed by coordination bonds.[4] The π-conjugation fully extended in two-dimensional plane, the redox property of the bis(diimino)nickel motif in a **NiDI** nanosheet, and the π–π overlap between the layers would be attributed to the electronic conduction in the bulk **NiDI** nanosheet.

2.5.3. Magnetic Properties

Magnetic properties of the **NiDI** CONASH were investigated using superconducting quantum interference device (SQUID). Some sample batch dependence was confirmed but all of the data exhibited non-negligible magnetic moments that did not follow the Curie-Weiss law. The data of a particular sample is shown in Fig. 2-15. χT decreases linearly with temperature down to 30 K, then rapidly decreases at lower temperature. The experimental susceptibility data could be simulated by considering temperature-independent term χ_0 in addition to the Curie-Weiss term according the formula: $\chi(T) = C_0(T - \theta)^{-1} + \chi_0$. The fitting from 2 K to 400 K afforded Curie constant $C_0 = 0.12$ cm^3·K·mol^{-1} and Weiss temperature $\theta = -3.0$ K. The Curie term suggests the existence of local magnetic moments and the negative θ value indicates the antiferromagnetic interaction between the spins in the **NiDI** sample. χ_0 can correspond to either the Pauli paramagnetism or Van Vleck paramagnetism, or a combination of both terms.

These results are intriguing because the neutral Ni(isq)$_2$, a fundamental constituted unit of the **NiDI** nanosheet, forms a non-magnetic singlet state owing to the strong antiferromagnetic coupling between the two S = 1/2 spins.[5] It is assumed that these observations are caused by randomness of the interlayer hydrogen bonding which resulted in a less ordered stacking of the **NiDI** nanosheets. The hydrogen bonding through the NH moieties is expected to perturb the singlet biradical characteristics of the Ni(isq)$_2$ unit to give rise to localized magnetic moments and conducting carriers, whose intensity/magnitude would be directly affected by the stacking (hydrogen-
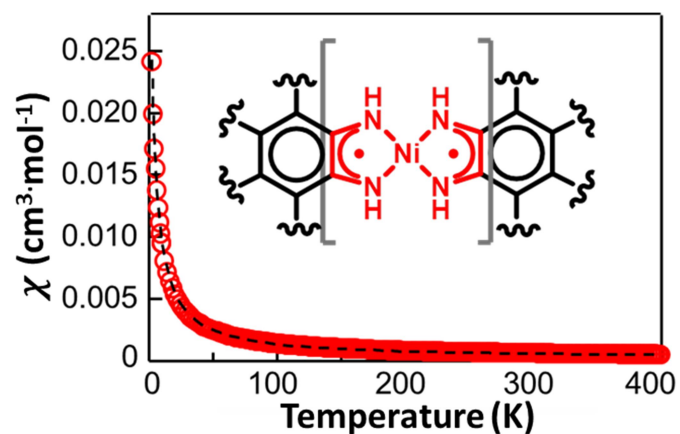
Fig. 2-15: Temperature-dependent magnetic susceptibility of **NiDI** CONASH. The dotted line is the fitting curve of $\chi(T) = C_0(T - \theta)^{-1} + \chi_0$ using the parameter $\chi_0 = 1.9 \times 10^{-4}$ cm³·mol⁻¹, $C_0 = 0.12$ cm³·K·mol⁻¹ and θ = -3.0 K. Inset shows a $C_4H_4N_4Ni$ magnetic unit.

bonding) pattern. However, more investigations regarding the magnetic properties are needed before deductions that are more conclusive can be made.

2.6.   Band Structure Calculations

The band structure for single layer, bilayer, and bulk **NiDI** were calculated using DFT first-principles methods, as implemented in Vienna *ab initio* simulation package. The projected augmented wave and the generalized gradient approximation[6] exchange-correlation potentials were used. For the bulk calculation, experimental crystal lattice parameters of $a = b = 13.01$ Å and $c = 3.25$ Å, as obtained from PXRD results, were adopted. For the single layer and bilayer calculation, the same lattice constants a and b were adopted with a vacuum layer thicker than 15 Å along the z direction to eliminate the interaction between the other layers. The Brillouin zone sampling was set as $7 \times 7 \times 9$ and $11 \times 11 \times 1$ for the bulk and layer calculations, respectively. The plane wave cut-off energy was set to 400 eV and the structural relaxations were carried out until the force on each atom was less than 0.02 eV·Å^{-1}.

The band structure of monolayer and bilayer **NiDI** is similar, as seen from Fig. 2-16(a) and (b), which shows metallic behaviour with the conduction band mainly formed by π-conjugated p_z orbitals from carbon and nitrogen. The band structure of bulk **NiDI** is displayed in Fig. 2-16(c) with the corresponding Brillouin zone and high-symmetry k-points depicted in Fig. 2-16(d). Unlike the weak van der Waals interaction, such as that between graphene layers, the π–π interaction between the **NiDI** layers is rather strong, as indicated by the interlayer band structure (blue region from Γ to A), which contributes to an interlayer electronic conductivity. The intrinsic bulk **NiDI** also shows a metallic feature like the layered nanosheets. However, with different oxidation or reduction environments, the location of the Fermi level can be changed, which in turn changes the electrical properties. This is especially when the Fermi level is moved into the two intra-layer gap regions (grey regions) by proper doping; the intra layer **NiDI** conduction changes from metallic to semiconducting, which suggests the possibility to tune the conductivity similar to **NiDT** CONASH.
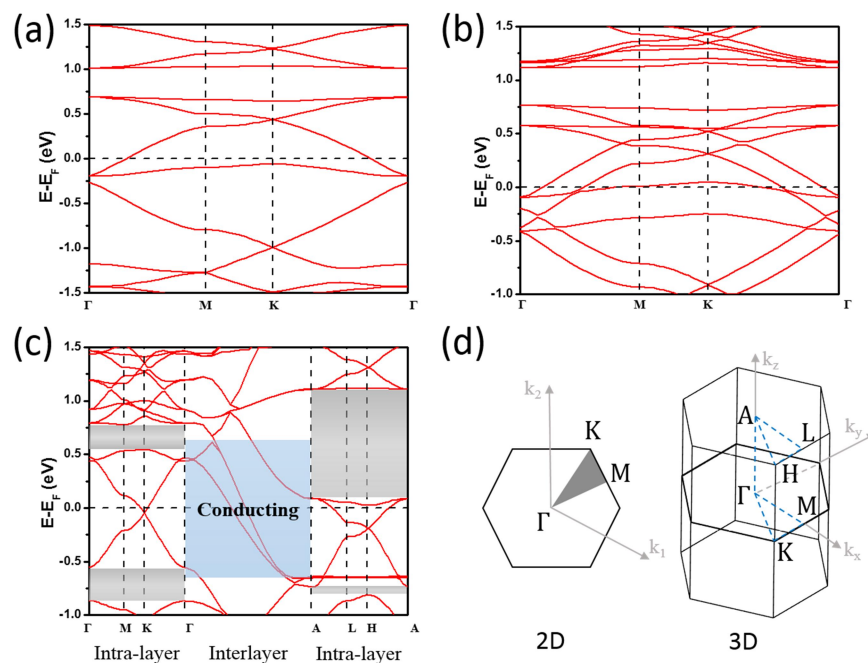
Fig. 2-16: First-principles band structures of NiDI (a) monolayer, (b) bilayer, and (c) bulk **NiDI**, where the grey regions indicate the intra-layer bandgap and the blue region indicates the interlayer conducting. (d) The first Brillouin zone and high-symmetry K-points for the layered and bulk systems, respectively.

2.7. Discussion

As of the time of writing, two other groups have also published their research on this particular system. However, their synthetic approach and properties of their material were found to be slightly different. In this section, some comparisons between both reported methods will be briefly discussed.

The first paper was reported by Lahiri *et al.*, who synthesized their films in a surprisingly similar method to that of the initial studies of this work.[7] Ethyl acetate solution of nickel(II) acetylacetonate was layered onto a degassed aqueous **HAB**·3HCl solution and then left to stand for 4 hours under atmospheric conditions. The difference between their method and the initial studies of this work is that sodium bromide was also added into the aqueous system. The resulting film was also an anionic one, with Na$^+$ ions as counter ions, as confirmed by XPS. Also, by exposing their setup under ambient atmospheric conditions the authors inadvertently but unexpectedly used molecular oxygen as an oxidant to synthesize the desired nanofilms. In addition, the authors also described the fabrication of devices using their films. Interestingly, it was reported that these devices were insulating, with resistivities in the range of GΩ, which is significantly different from the semiconductive properties of **NiDI** found in this work.

Dou *et al.* then published their research using their own method of synthesis, which included warming solution mixtures of water and dimethylsulfoxide, up to 60 °C.[8] It was reported that the film they obtained is neutral and also noted the important role of oxygen for the reaction. However, they concluded that their obtained nanosheet has a slipped parallel structure (CmCm space group) rather than an eclipsed structure (P6/mmm space group).

The difference in reaction temperature might cause a difference in crystalline film growth rate, which resulted in the absence of peak [041] from Dou's structure for our nanosheet in the powder XRD pattern. Thus, our calculated band structure is based on an eclipsed structure. Since the calculated band structure is different, it is reasonable to rationalize that the resulting band structure would also be different. Comparatively,

both calculations strongly suggest a metallic nature of bulk **NiDI**, even though both groups observed semiconducting behaviour. This could be attributed to the thermally activated hopping of carriers between grain boundaries since a pelletized sample was used.

2.8.   Conclusion

A novel redox active **NiDI** nanosheet has been synthesized using a new kind of gas/liquid interfacial reaction under mild conditions. By utilizing molecular oxygen to generate radicals during the coordination reaction, the exposure to atmospheric oxygen on the surface allows for a slow diffusion and slow formation of the nanosheets, which in turn, led to the formation of large crystalline nanosheets on a calm liquid interface. Previous synthetic protocols typically require sacrificial radical-containing/generating compounds, which usually involve stirring the reaction mixtures. Although such mechanical agitation is effective, it requires a longer reaction time, and thus smaller nanosheets are obtained. The new slow diffusion layering method is independent of mechanical stirring, which enables the formation of very large nanosheets. In fact, the only limitation to the size of nanosheet formed would be the size of the reaction vessel used, as that determines the surface area of the solution exposed for oxidation.

This **NiDI** nanosheet is also potentially useful for many applications in the future such as electronic devices since it exhibited electron-conducting properties. Interesting magnetic data has also been obtained, although yet to be fully explained. Band structure calculations also suggest the possibility of tuning physical properties of the **NiDI**, such as its conductivity, by using doping or redox reactions.

2.9.   Experimental Section

FT-IR spectra were recorded using a JASCO FT/IR-6100 at room temperature under vacuum using a KBr pellet. Surface IR (ATR) was recorded using ThermoFisher Nicolet iS-50 FT-IR. ^{1}H (500 MHz) NMR spectra were recorded on a Bruker-DRX500 spectrometer. Powder X-ray diffraction (pXRD) pattern of chemically synthesized **NiDI** was obtained using synchrotron radiation (λ = 0.80 Å) at Beamline BL02B2, at Super Photon ring-8 GeV (SPring-8) in Japan. The sample was ground finely packed into a 0.5 mm-diameter soda tube.

Field Emission-Scanning Electron Microscopy images were collected using a JEOL JSM-7400FNT equipped with an EDS analyzer (JEOL EX-2300). TEM images were recorded at 75 kV using a Hitachi HF-2000 equipped with an AMT-CCD camera. X-ray Photoelectron Spectroscopy data were obtained using PHI 5000 VersaProbe (ULVAC-PHI, INC.). Al Kα (15 kV, 25 W) was used as the X-ray source, and the beam was focused on a 100 μm^2 area. The spectra were analysed using the MultiPak Software and standardized using a C1s peak at 284.6 eV. Atomic Force Microscopy (AFM) was carried out using an Agilent Technologies 5500 Scanning Probe Microscope, under ambient conditions, in the high-amplitude mode (tapping mode), with silicon cantilever PPP-NCL (Nano World). DFT calculations were performed on Gaussian 09. PXRD simulations were calculated on CrystalDiffract program.

Cyclic voltammetry used a three-electrode configuration electrochemical cell with 1 M acetonitrile solution of tetrabutylammonium hexafluorophosphate as the electrolyte solution, a Pt coil as the counter electrode and an Ag$^+$/Ag electrode as the reference electrode. Their set ups were monitored by the 650DT electrochemical analyzers. (BAS Co., Ltd.) The reported potentials were adjusted from Ag$^+$/Ag to Fc$^+$/Fc using the difference in potentials between the two redox couples.

For substrate preparations, Highly Ordered Pyrolytic Graphite (HOPG) was obtained from Alliance Biosystems, Inc. (Grade SPI-1/2 10 × 10 × 2 mm) and its surface renewed with adhesive tape just before use. Silicon wafers (P-doped with a

concentration of 3×10^{18} cm^{-3}) with thermally grown 100 nm-thick SiO$_2$ were purchased from Yamanaka Semiconductor, and cut into 12 mm by 12 mm small squares. Hexamethyldisilazane (HMDS) treatment was then carried out by submerging the silicon wafers in an ethanol solution (10 mL) of HMDS (100 μL) for 1 day. After rinsing with ethanol, the wafers were annealed at 120 ^{o}C for 2 hours and then dried under vacuum.

Band structure calculations were carried out kindly by Liu's group from University of Utah. The band structure for single layer and bulk **NiDI** were calculated using DFT first-principles methods as implemented in Vienna *ab initio* simulation package. For the bulk calculation, experimental crystal lattice parameters of $a = b = $ 13.01 Å and $c = 3.25$ Å, as obtained from PXRD results, were adopted. For the single layer calculation, we adopted the same lattice constants a and b with a vacuum layer thicker than 15 Å along the z direction to eliminate the interaction between the other layers. The Brillouin zone sampling was set as $7 \times 7 \times 9$ and $11 \times 11 \times 1$ for the bulk and layer calculations, respectively. The plane wave cut-off energy was set to 400 eV and the structural relaxations were carried out until the force on each atom was less than 0.02 eV·Å^{-1}.

For the conductivity measurements, the **NiDI** obtained from vacuum filtration were first ground using a mortar and pestle before pressing into a pellet. The pelletized form was then approximately sliced into flat rectangular strips for the resistivity measurements. The direct-current resistivity measurements were performed with the pelletized **NiDI** using the standard four-probe method. Electrical contacts were obtained by gluing four gold wires (15 μm diameter) to the pellet with carbon paste.

The temperature dependencies of the magnetic susceptibilities of **NiDI** were measured with a Quantum Design MPMS SQUID magnetometer. Aluminium foil was used as a sample container; its magnetic contribution was subtracted as background by measuring its own magnetic susceptibilities during every measurement.

2.9.1. Synthesis of Ligand

The chemicals were bought commercially and used without any further purification from Kanto Chemical Co. Inc., Sigma-Aldrich Co. and Wako Pure Chemical Industries Ltd. Dry solvents were purified with a Glass Contour Solvent Dispensing System (Nikko Hansen & Co., Ltd.). Water was purified using the Milli-Q purification system (Merck KGaA).

Hexaaminobenzene trihydrochloride (**HAB**·3HCl) was synthesized using slightly modified literature procedures according to the scheme as shown in Fig 2-17.[9]
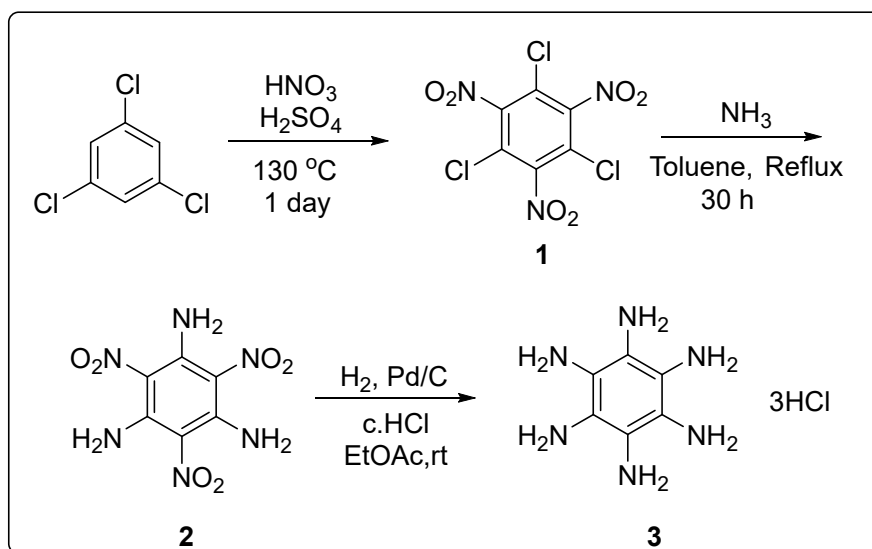
Fig. 2-17: Synthetic scheme for hexaaminobenzene trihydrochloride ligand.

Synthesis of 1,3,5-Trichloro-2,4,6-trinitrobenzene (1)

Fuming nitric acid (4.9 mL, 112 mmol) was added slowly to a stirring solution of fuming sulfuric acid (50%, 250 mL) at 0 °C. After the addition was complete, the ice-bath was removed and a condenser was equipped, and then the mixture was heated to 80 °C. The precursor, 1,3,5-trichlorobenzene (20.3 g, 22.4 mmol), was added portion wise and then the temperature was raised to 130 °C and left overnight. The reaction mixture was then allowed to cool to room temperature and then poured onto roughly 300 mL of ice. The resulting solid was vacuum filtered and then washed with water and

diethyl ether, respectively. The resulting white solid, **1**, (5.09 g, 72%) was >95% purity by gas chromatography mass spectroscopy. The slight impurity was found to be tetrachlorodinitrobenzene. IR (ATR, cm^{-1}): υ 1546, 1343, 951, 848. MS (GCMS): 315 [M]$^{+}$.

Synthesis of 1,3,5-Triamino-2,4,6-trinitrobenzene (2)

Compound **1**, 1,3,5-trichloro-2,4,6-trinitrobenzene (4.34 g, 13.7 mmol) was dissolved in toluene (90 mL). Anhydrous ammonia was bubbled through the solution heated under reflux for 30 h. After being cooled to room temperature, the resulting mixture was filtered. The yellow residue was washed with toluene, acetone and water until the solvents ran clear and finally with some acetone once again to dry the final yellow solid, **2** (2.73 g, 77%). IR (ATR, cm^{-1}): υ 3316, 3216, 1612, 1568, 1446, 1321, 1222, 1176, 1028. MS (EI): 258 [M]$^{+}$.

Synthesis of Hexaaminobenzene Trihydrochloride (3)

Triaminotrinitrobenzene (**2**) (503.5 mg, 1.95 mmol) was placed in a 50 mL Schlenk flask together with 10% Pd/C (90 mg) and dry EtOAc (50 mL) as a solvent and the joints were sealed tightly. The air in the reaction flask was removed with a quick vacuum without evaporating too much of EtOAc and replaced with H$_2$ gas from a balloon. The reaction was left to stir for 2 days, with the H$_2$ balloon replaced when the pressure of the balloon decreased. Then, concentrated hydrochloric acid (15 mL) was added to the system, and the reaction was continued under H$_2$ for an additional 3.5 h. The colour of the mixture would have changed from black to slightly grey. The reaction mixture was filtered under reduced pressure over Celite to remove catalyst. About 50 mL of 1 M hydrochloric acid (HCl) was then used to wash the solids. The hexaaminobenzene trihydrochloride then crystallized out in the filtrate. More concentrated HCl is added to the filtrate to encourage recrystallization. The white or pale pink solids were collected by suction filtration by using polytetrafluoroethylene (PTFE) membrane (0.5 μm pore) and washed thoroughly with EtOAc and dried to afford 415.8 mg of **3** (77% yield). The product was kept in tightly sealed vials under

argon. IR (KBr, cm^{-1}): υ 3384, 3249, 2977, 2565, 1671, 1636, 1582, 1554, 1480, 1279, 1203, 1166, 1096.

2.9.2. *Synthesis of Nanosheets*

0.05 M of aqueous nickel(II) acetate solution was prepared with degassed water and an equivalent amount of concentrated aqueous ammonia was added. 15 mL of the resulting deep blue solution was then added to 10 mL of 1 mM of aqueous ligand solution under argon atmosphere in a 50 mL vial. The vial and its resulting solution were then exposed to atmospheric air at room temperature, with the duration controlled if thinner sheets are required. The shiny black film formed on the aqeuous surface was the **NiDI**. In the case of thinner **NiDI** sheets, the sheets were collected and transferred under argon atmosphere with exposure to atmospheric air ranging from 1 to 5 hours.

2.10. References

1. (a) T. Kambe, R. Sakamoto, K. Hoshiko, K. Takada, M. Miyachi, J.-H. Ryu, S. Sasaki, J. Kim, K. Nakazato, M. Takata, H. Nishihara, *J. Am. Chem. Soc.*, **2013**, *135*, 2462-5.
   (b) T. Kambe, R. Sakamoto, T. Kusamoto, T. Pal, N. Fukui, T. Shimojima, Z. Wang, T. Hirahara, K. Ishizaka, S. Hasegawa, F. Liu, H. Nishihara, *J. Am. Chem. Soc.*, **2014**, *136*, 14357-60.

2. (a) D. Herebian, E. Bothe, F. Neese, T. Weyhermüller, K. Wieghardt, *J. Am. Chem. Soc.*, **2003**, *125*, 9116-28.
   (b) J. Ciccione, N. Leconte, D. Luneau, C. Philouze, F. Thomas, *Inorg. Chem.*, **2016,** *55*, 649–65.

3. D. Sheberla, L. Sun, M. A. Blood-Forsythe, S. Er, C. R. Wade, C. K. Brozek, A. Aspuru-Guzik, M. Dincă, *J. Am. Chem. Soc.*, **2014***, 136,* 8859-62.

4. (a) F. Gándara, F. J. Uribe-Romo, D. K. Britt, H. Furukawa, L. Lei, R. Cheng, X. Duan, M. O'Keeffe, O. M. Yaghi, *Chem. Eur. J.*, **2012**, *18,* 10595.
   (b) Y. Kobayashi, B. Jacobs, M. D. Allendorf, J. R. Long, *Chem. Mater.*, **2010**, *22*, 4120.
   (c) A. A. Talin, A. Centrone, A. C. Ford, M. E. Foster, V. Stavila, P. Haney, R. A. Kinney, V. Szalai, F. El Gabaly, H. P. Yoon, F. Leonard, M. D. Allendorf, *Science,* **2014**, *343,* 66.

5. D. Herebian, K. E. Wieghardt, F. Neese, *J. Am. Chem. Soc.*, **2003**, *125*, 10997–1005.

6. (a) G. Kresse, D. Joubert, *Phys. Rev. B.*, **1999**, *59*, 1758-75.
   (b) J. P. Perdew, W. Yue, *Phys. Rev. B.*, **1986**, *33,* 8800-2.

7. N. Lahiri, N. Lotfizadeh, R. Tsuchikawa, V. V. Deshpande, J. Louie, *J. Am. Chem. Soc.*, **2017**, *139*, 19−22.

8. J.-H. Dou, L. Sun, Y. Ge, W. Li, C. H. Hendon, J. Li, S. Gul, J. Yano, E. A. Stach, M. Dincă, *J. Am. Chem. Soc.*, **2017**, *139*, 13608–11.

9. (a) Z.-G. Tao, X. Zhao, X. K. Jiang, Z.-T. Li, *Tetra. Lett.,* **2012**, *53*, 1840.
   (b) J. Mahmood, D. Kim, I.-Y. Jeon, M. S. Lah, J.-B. Baek, *Synlett.*, **2012**, *24*, 246.

Chapter 3

ELECTROCHEMICAL
BIS(DIIMINO)NICKEL(II) NANOSHEETS

3   ELECTROCHEMICAL BIS(DIIMINO)NICKEL(II) NANOSHEETS

3.1.   Introduction

In Chapter 2, a new method for the synthesis of **NiDI** which skilfully makes use of oxygen to obtain relatively large and crystalline sheets has been developed. This method however, requires a relatively long time without a qualitative control. Furthermore, due to the prevalence of N-H bonds in the **NiDI** sample, hydrogen bonding can sometimes causes the difficulty of adsorption onto the substrates we want to transfer to. The **NiDI** film which is being formed on an aqueous surface, forms strong hydrogen bonding with water molecules. During the transfer, small amounts of water molecules are trapped between the sample and the substrate surface. This sometimes causes the detachment of the **NiDI** film from its substrate when the sample is being dried. An example can be seen in Fig. 2-4, where the **NiDI** film on the glass substrate is not lying flat on the substrate but is standing in air.

In the exploration of methods to adsorb our samples tightly onto substrates, we developed the electrochemical method of synthesis which also utilizes oxidation but in another form of removing electrons. This method synthesizes the **NiDI** directly onto an electrode surface, so the adhesion of the film is not a point of consideration anymore. This also adds another advantage as compared to films transferred onto substrates, as being synthesized directly on the substrate means the reduction of air or water molecules that can contribute to a slight increase in resistance between the sample and substrate. Furthermore, using the electrochemical method, we are able to control the amount of charge supplied to the system which is used to oxidize the reagents and hence control the amount of **NiDI** CONASH formed.

3.2. Synthesis of Electrochemical NiDI

Discovering the necessity for oxidation, another synthetic method using electrochemical oxidation was developed, which produces the **NiDI** nanosheet directly on an electrode surface. The electrochemical polymerization was carried out at an indium-tin oxide (ITO) glass in a **HAB**·3HCl-Ni(OAc)$_2$-NH$_3$ aqueous solution with 0.1 M NaBF$_4$ as electrolyte under an argon atmosphere as illustrated in Fig. 3-1. A black film immediately formed and adhered strongly to the ITO electrode when a constant potential of 0.56 V vs. Ag/AgCl was applied to oxidize the **HAB**. In comparison, electro-oxidation of nickel-free reaction solution (**HAB**·3HCl-NH$_3$-NaBF$_4$) afforded no film on the electrode, indicating the role of nickel ions for the polymerization.
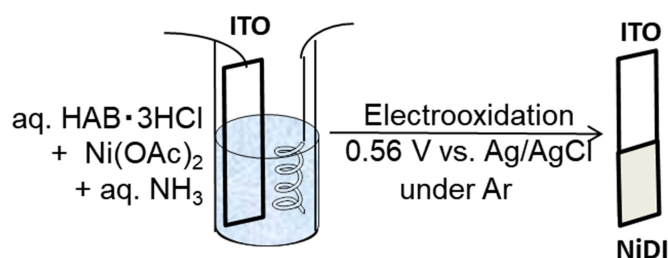
Fig. 3-1: Illustration of the synthetic set up for electrochemical synthesis of **NiDI**.
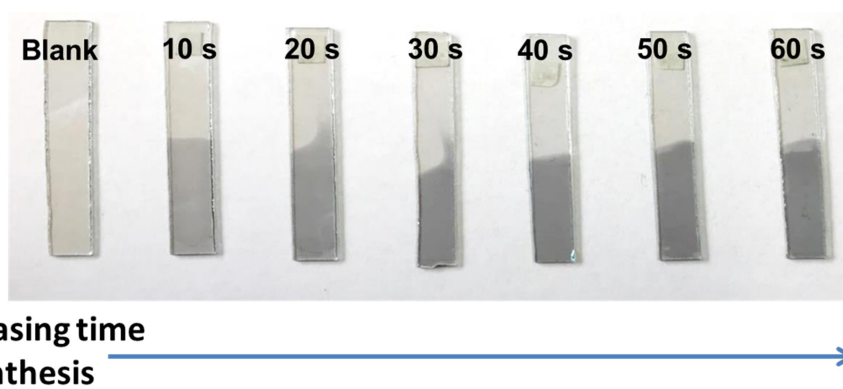
Fig. 3-2: Photograph of samples of **NiDI** on ITO with increasing synthetic time.

This electrochemical method enables a more controllable growth of the nanosheet as compared to the gas-liquid interfacial reaction as the degree of oxidation can be precisely adjusted. A series of samples with synthetic times varying from 10 s to 60 s can be synthesized as seen in Fig. 3-2. It can be seen that the amount of **NiDI**

formed on the ITO substrate increases with the increase in synthetic time as indicated by the increasing opacity with time.

As the chemistry of the **NiDI** formation is the same, it is postulated that the same reaction mechanism as described in section 2.3 and illustrated in Fig. 2-6 is applicable for the electrochemical synthesis of **NiDI**.

3.3. Characterization

3.3.1. X-ray photoelectron spectroscopy (XPS)
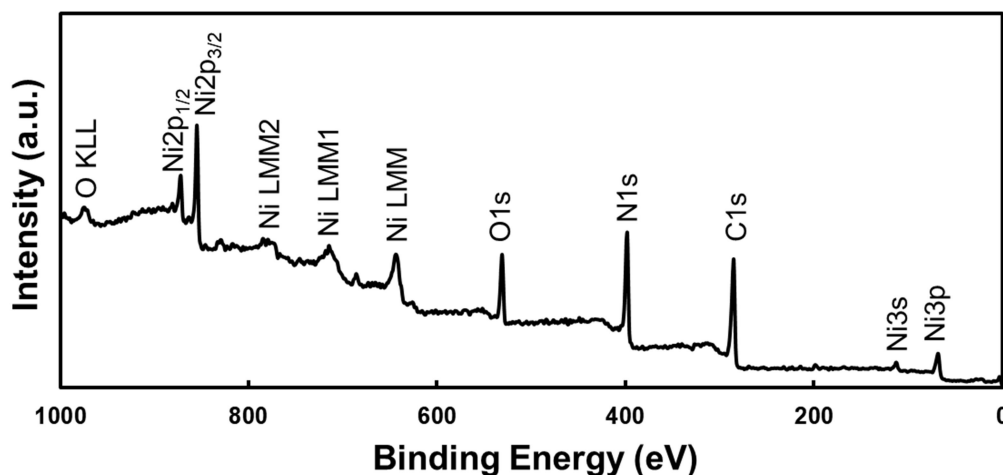
Fig. 3-3: XPS spectrum of neutral **NiDI** films formed by the electrochemical method.

The electrochemically synthesized **NiDI** sheets were characterized using X-ray photoelectron spectroscopy (XPS) as seen in Fig. 3-3 and the wide spectrum showed the similar presence of N1s, Ni2p, and C1s peaks to the chemically synthesized **NiDI** nanosheet (Fig. 2-7). The elemental ratio of nickel to nitrogen was also found to be 1:4, same as the expected ratio. From the XPS spectrum, since no other cations or anions could be formed from the reagents used, it is concluded that a neutral form of **NiDI** has been obtained similarly using this new synthetic method.

Also, when the high resolution XPS spectra of the two types of **NiDI** are compared in Fig. 3-4, it can be seen that both types of **NiDI** show peaks with similar binding energies. This further proves that the **NiDI** formed by the two methods are identical in terms of their composition.
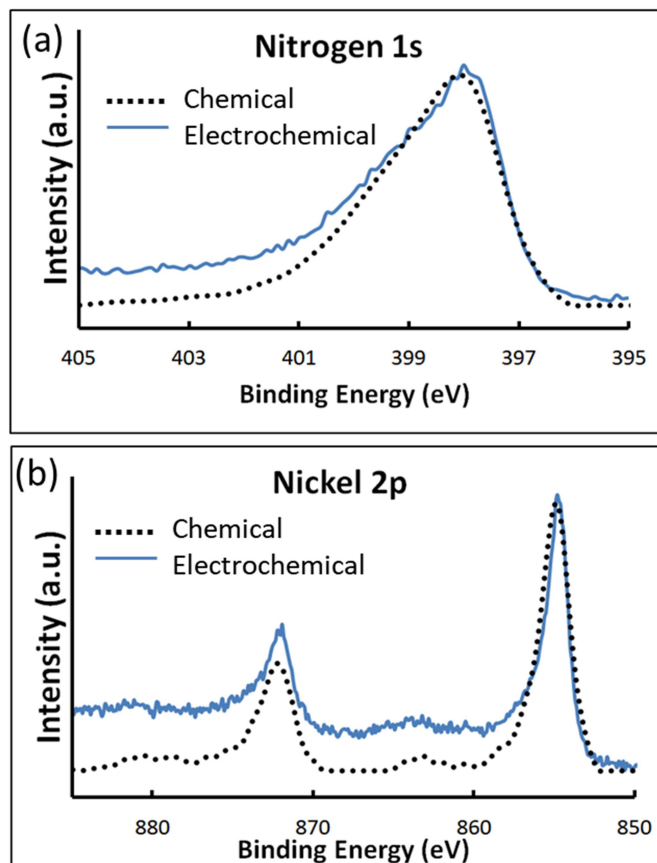
Fig. 3-4: Comparison of high resolution XPS spectra of chemical and electrochemical **NiDI**. (a) and (b) shows high resolution XPS spectra of both samples in the nitrogen 1s and nickel 2p regions respectively.

3.3.2 Infrared spectroscopy

Solid KBr infrared spectroscopy of the electrochemically synthesized **NiDI** in Fig. 3-5 gave distinct bands and these are similar to the spectrum of the chemically synthesized **NiDI**. The band at about 3200 cm^{-1} is assigned to the N-H stretching band (purple), the peak at approximately 1600 cm^{-1} can be assigned to be signal from the aromatic ring (green) while the strong signal at about 1400 cm^{-1} match with the C-N stretching band (orange). These bands from infrared spectroscopy further prove that the structure of the electrochemically synthesized **NiDI** nanosheet is the similar to that of the chemically synthesized as described in Chapter 2.

.
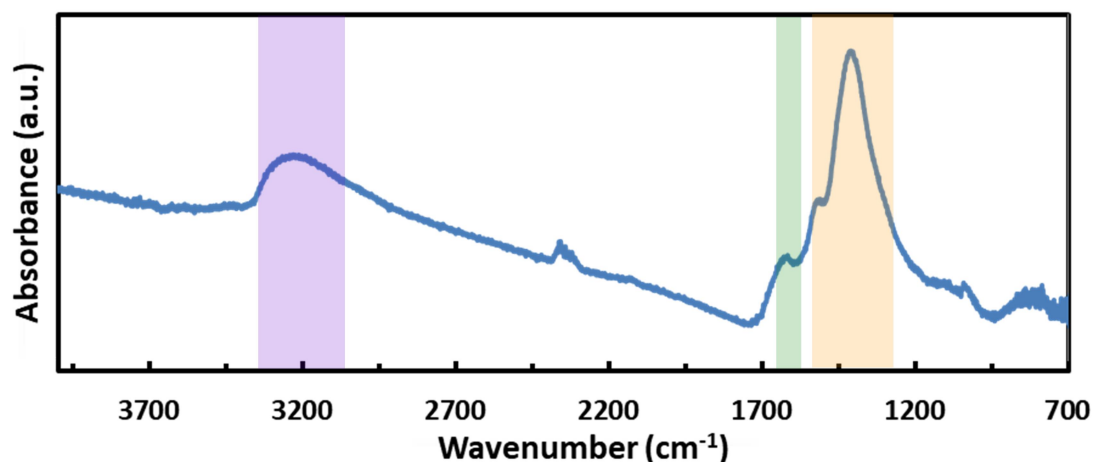
Fig. 3-5: IR spectrum of electrochemically synthesized **NIDI**.

3.3.3 *Powder X-ray Diffraction*

Powder X-ray diffraction (PXRD) analysis of the electrochemically synthesized **NiDI** sheet obtained using high energy synchrotron radiation (λ = 1.08 Å) gave some broad peaks, which shows that this method give products with crystallinity much lower than that of the chemically synthesized **NiDI**. The less ordered structure of electrochemically prepared **NiDI** is, however, understandable as it results from the quick formation and the difference of the reaction field (solid-liquid interface for the electropolymerization versus gas-liquid interface for the chemical polymerization).

These peaks obtained, as seen in Fig. 3-6(a), were found to also match the simulation data of an eclipsed nanosheet array with the crystal lattice parameters of $a = b = 13.01$ Å and $c = 3.25$ Å. The three relatively obvious peaks at $2\theta = 5.5°$, $11.0°$ and $19.0°$ were found to match to the [100], [200] and [001] diffraction planes respectively.

Although the simulated pattern of the **NiDI** sheet stacked in a staggered pattern as shown in Fig. 3-6(b) also have corresponding peaks at similar positions for diffraction planes [100], [011] and [002], it was concluded to be less matched as compared to the eclipsed form to the experimental data. This is due to the absence of the [201] diffraction peak which should appear at about $14.5°$, which if present, should give a peak of slightly lower intensity to the peak at $11.0°$.
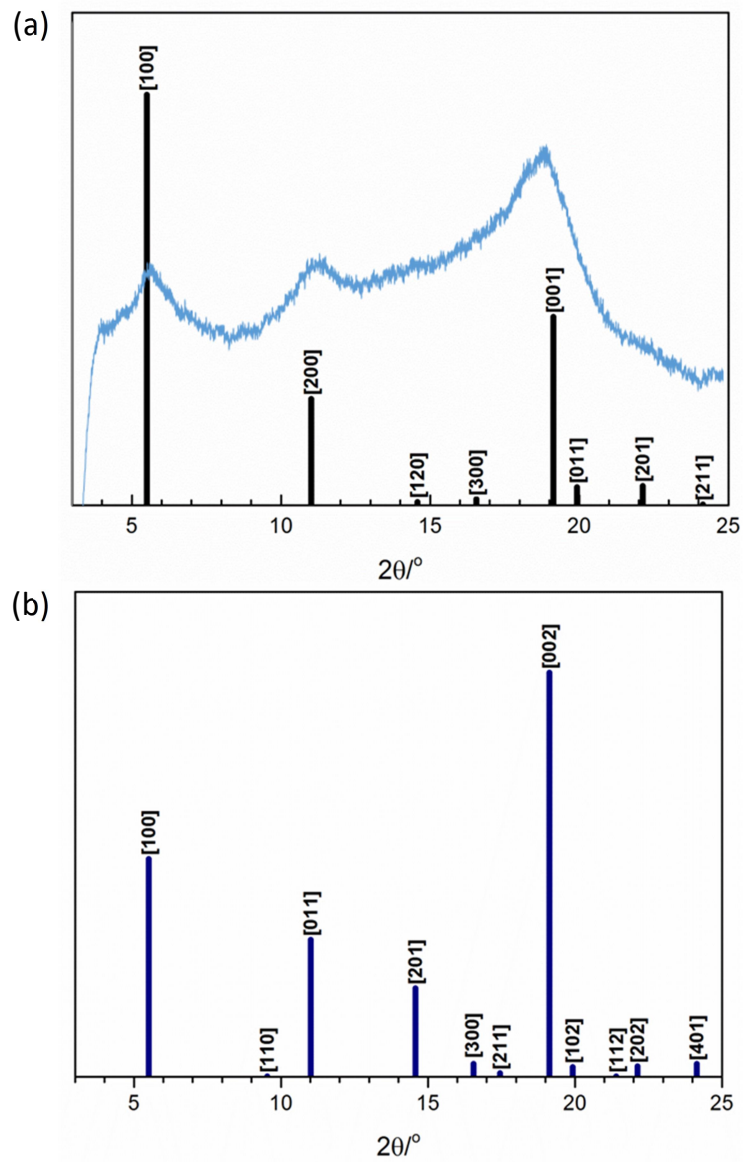
Fig. 3-6: Powder XRD spectrum ($\lambda = 1.08$ Å) of experimental **NiDI** (blue) matching with simulated spectrum of (a) eclipsed **NiDI** and (b) staggered **NiDI**.

3.4.   Time as a Variable

Using time as a variable, several **NiDI** samples on ITO have been synthesized to obtain different amounts of **NiDI** on the electrodes. As pictured in Fig. 3-2, the longer time the ITO electrode is exposed to the constant potential, the more **NiDI** is deposited as seen from the increasing opacity with time. Using these **NiDI** samples with a time variable of 10 s to 60 s, some new properties of the **NiDI** CONASH was investigated.

3.4.1. *Ultraviolet-visible-near infrared Spectroscopy*

Electronic data was previously not really obtainable using the chemical **NiDI** as the CONASH obtained did not adsorb well on the electrodes. The thicker sheets which are able to adsorb well on the substrates are usually too opaque to be measured.

This electrochemical method enables a more controllable growth of the nanosheet as compared to the gas-liquid interfacial reaction as the degree of oxidation can be precisely adjusted. Fig. 3-7 shows the UV-vis-NIR spectra of six different samples obtained by applying a constant potential of 0.56 V vs Ag/AgCl in a **HAB**·3HCl-Ni(OAc)$_2$-NH$_3$ aqueous solution with 0.1 M NaBF$_4$ under argon atmosphere for 10 s to 60 s, respectively.
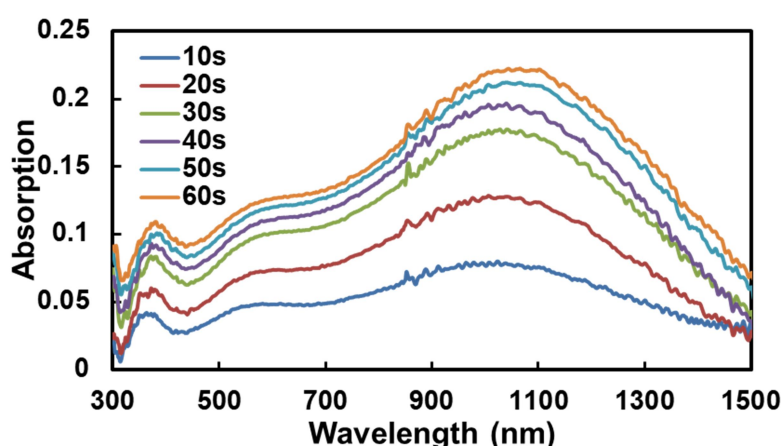
Fig. 3-7: UV-vis-NIR spectra of electrochemically synthesized **NIDI** by constant potential electrolysis at 0.56 V vs Ag/AgCl in a **HAB**·3HCl-Ni(OAc)$_2$-NH$_3$ aqueous solution with 0.1 M NaBF$_4$ under Ar for 10 s to 60 s respectively.

It can be observed that the absorbance increases with the synthetic time, which matches the observation of the increased opacity. However, when compared to similar nickel-amino based mononuclear compounds from past studies, the spectra are distinctively different.[1] This could be due to the extended delocalization of electrons in the polymeric structure. The spectra exhibit a broad peak over 700 – 1500 nm with λ_{max} = ca. 1060 nm and have a non-linear relationship with the synthetic time. This non-linear relationship would be further elaborated in a later section.

3.4.2. *Atomic Force Microscopy (AFM) images*

To investigate more into the structure and thicknesses of the **NiDI** formed on the ITO electrode as a comparison to the chemically synthesized **NiDI**, representative scratched samples with synthetic times of 20 s, 40 s and 60 s were observed under the AFM. The samples were scratched with a blade to expose a section of bare ITO such that a more accurate relative height of the **NiDI** deposited could be determined. The samples with longer synthetic time have thicker depositions are easier to scratch. It can be observed that the non-scratched regions of the samples show non-planar and jagged surfaces from their AFM topographical images as seen from Fig. 3-8. The scratched regions are as indicated in the topography images.
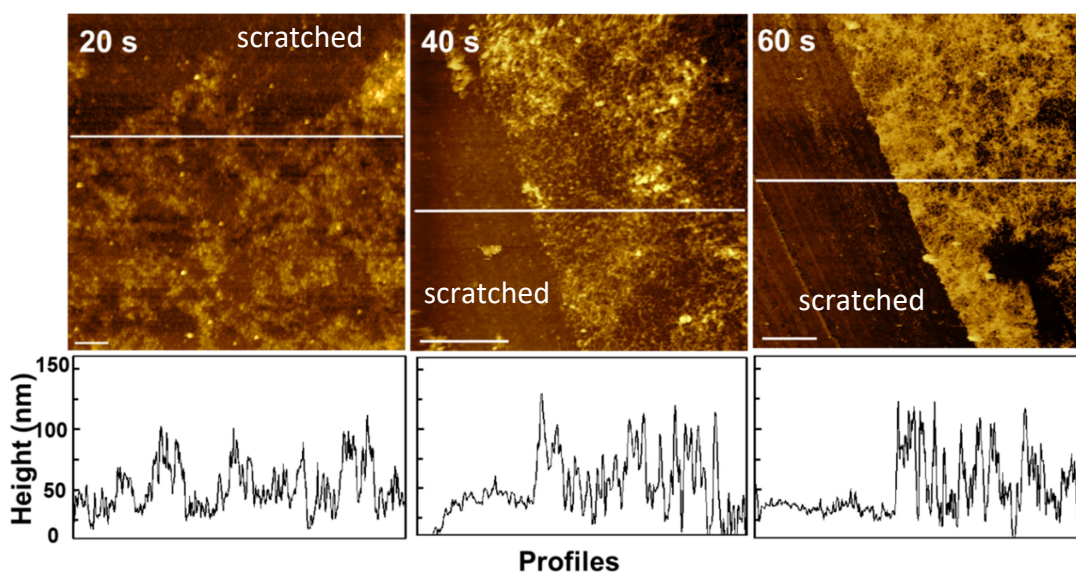
Fig. 3-8: AFM topography images and height profiles of scratched AFM samples obtained by 0.56 V for 20 s, 40 s and 60 s, respectively. Scale bars represent 5 μm.

As seen from the height profile, the empty spaces (blank ITO without **NiDI**) of the deposited CONASH at the non-scratched areas decreased while the topographical height increased gradually with time. After 60 s of synthesis, the average thickness of the NiDI film was 75 nm. As observed by the jagged height profiles, it seems to indicate the growth of perpendicularly deposited **NiDI** nanosheets. This is illustrated in Fig. 3-9 where the **NiDI** which are perpendicularly deposited on the ITO electrodes are gradually increasing in height and amount. The illustration of chemically synthesized **NiDI** using the interfacial method and then transferred parallel onto the substrates is also given as a comparison.
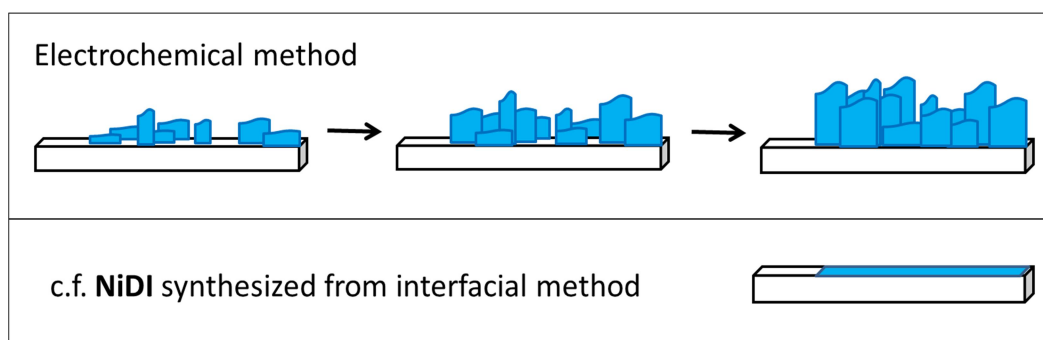
Fig. 3-9: Illustration of scratched **NiDI** samples on ITO with increasing synthetic time. The illustration of the chemical **NiDI** transferred onto substrates is given as a comparison.

3.4.3. *Cyclic Voltammetry*

Redox activities of the electrochemically synthesized **NiDI** nanosheets were investigated using cyclic voltammetry (CV) in 1 M Bu_4NClO_4-MeCN as electrolyte, Pt as counter electrode and Ag^+/Ag as reference electrode. The 20 s sample of the electrochemically synthesized **NIDI** on ITO was used directly for the measurement and the obtained data is given in Fig. 3-10. Comparing with Fig. 2-12 of the chemically synthesized **NiDI**, the **NiDI** nanosheet samples synthesized from both methods exhibit their peak couples at approximately 0.28 V vs. ferrocenium/ferrocene (Fc^+/Fc) with chemical reversibility. This peak couple can also be ascribed to $[\textbf{NiDI}]^+/[\textbf{NiDI}]^0$ based on the redox behaviour of the mononuclear bis(diimino)nickel complex.
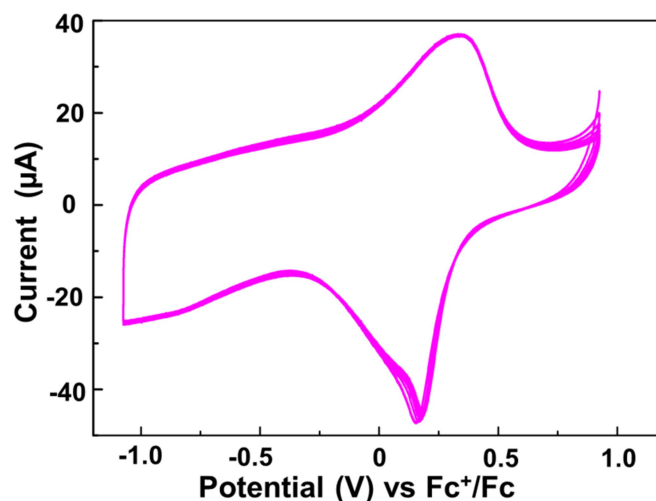
Fig. 3-10: Cyclic voltammogram of 20 s sample of electrochemically synthesized **NiDI** on ITO electrode.

Representative cyclic voltammograms of the electrochemically prepared **NiDI** on ITO were also plotted together in Fig 3-11 to show an increase in their charge capacity with the increase in synthetic time. This is especially obvious when the graphs are compared to the bare ITO which is unable to hold any charges.
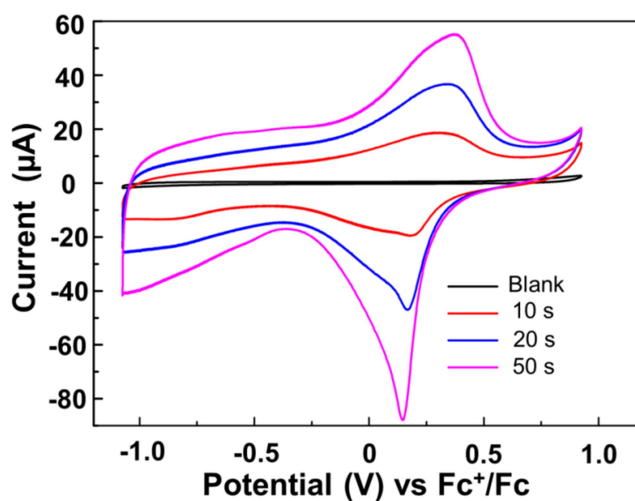
Fig. 3-11: Cyclic voltammograms showing increasing capacity of **NiDI** with increasing synthetic timings of 10 s, 20 s and 50 s respectively as compared to blank ITO.

This observation shows that there is an increase in charge capacity with the amount of **NiDI**. Together with its stable redox behaviour and electrical conductivity, this observation, which was not possible with the previous chemical method, reveals the potential of **NiDI** for charge storage applications.

3.5.   Discussion

The electrochemical method for the synthesis of **NiDI** has obvious advantages even though the resulting samples are not as crystalline. From the various characterizations, the samples with different amounts of **NiDI** could be compared, which was previously not possible using only the chemical method. These various findings also further revealed other characteristics of the **NiDI**-modified ITO electrodes.

Cyclic voltammograms of electrochemically prepared **NiDI** nanosheet on ITO exhibits not only faradaic currents but also very large charging currents. The amount of charge (labelled as charge A) gained from each sample with increasing synthetic durations during its CV has been plotted against time in Fig. 3-12. The absorbance of the respective samples at λ_{max} (1060 nm) and the gradual increase of the charge (labelled as charge B) consumed during their syntheses, using a 60 s sample as an example, were also plotted against the same time axis. Charge vs time graph for each of the respective samples during cyclic voltammetry. The three different sets of data all increases non-linearly with time and matches approximately to the same relationship.
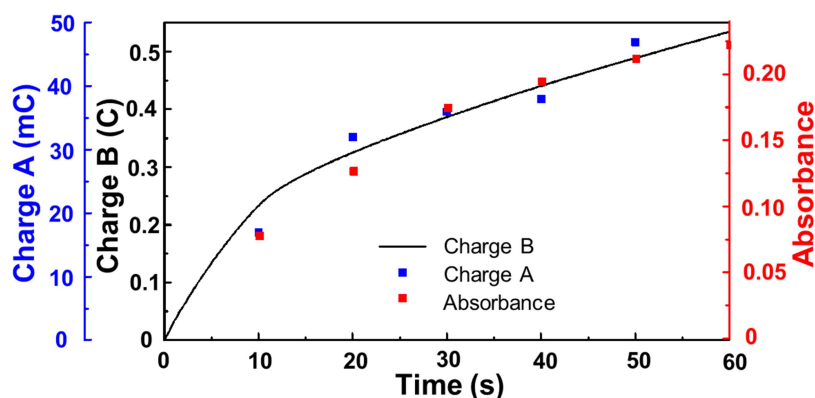
Fig. 3-12: Absorbance at λ_{max} of the samples synthesized by differing durations corresponding to the charge A, the electro activity charges, and charge B, the charge obtained during the synthesis of the sample with 60 s of 0.56 V vs Ag/AgCl constant potential.

This non-linear increase corresponds to the previous hypothesis of the perpendicular growth of **NiDI** on the ITO electrodes as described in the previous section. Charges A and B showing the same relationship indicates that the amount of charge that

each sample contains corresponds to the amount that is gained during the synthesis itself. This is also further proven in the absorption at λ_{max} which is indicative of the amount of **NiDI** on each of the electrodes. In other words, since the three sets of data correspond to each other, it means that the amount of charge that is absorbed during the synthesis of the sample has all been used up for the synthesis of the compound, deposited onto the ITO electrodes, and all of the **NiDI** formed has also remained attached on the electrodes.

One other comparison would be between the cyclic voltammograms of the chemical and electrochemical **NiDI** samples. It has already been mentioned that both the **NiDI** nanosheet samples exhibit the peak couples at approximately 0.28 V vs. ferrocenium/ferrocene (Fc$^+$/Fc). However, there is a slight difference between the potential difference of the oxidation and reduction peaks for the two types of samples.

Fig. 3-13 shows the cyclic voltammograms of both samples stacked together on the same potential axis vs ferrocenium/ferrocene. The highlighted regions represent the difference in potentials for each sample in their representative colours. It can be observed that the black region indicating the potential difference for the electrochemical sample is much smaller than the red region representing the chemical sample.
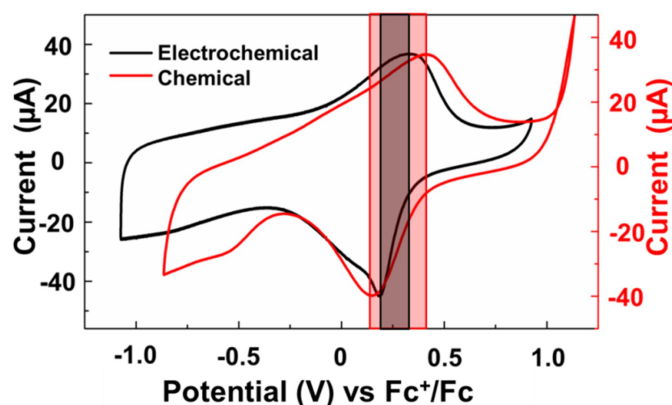
Fig. 3-13: Cyclic voltammograms of both the electrochemical and chemical **NiDI** samples. The coloured regions highlight the potential difference between oxidation and reduction potentials for each type of sample in their respective colors.

This smaller difference in the potential difference essentially indicates a smaller electroresistance between the sample and the substrate for the electrochemical **NiDI** sample on ITO. This is to be expected since the **NiDI** CONASH has been synthesized directly onto the ITO electrode while transferred films could potentially contain water molecules or just a thin layer of air between the film and substrate, thus increasing the resistance. Although the difference is not too great, a lower amount of resistance is more advantageous if the **NiDI** material is eventually utilized for applications such as charge storage devices.

3.6.   Conclusion

Two separate methods of slow oxidation and controlled oxidation have been successfully used to synthesize and characterize **NiDI**. The initial chemical method was useful to obtain structure information since the resulting CONASH was relatively more crystalline. The electrochemical method described in this chapter proved to give the same **NiDI** product with a slight difference in the eventual orientation of the sheets on the substrates when compared with the chemically synthesized samples.

The electrochemically synthesized **NiDI** samples also gave an additional option of investigating the change in properties of the samples with increasing amounts of **NiDI**. Absorption spectra and cyclic voltammograms of samples with gradual increasing amounts of **NiDI** synthesized under a minute found that all the charges used in the electrochemical synthesis were used to oxidize and form the product and the resulting CONASH was all directly attached to the ITO electrode used. The potential of this material as a charge storage material and an additional advantage over the chemical **NiDI** in device applications was also revealed though this electrochemical method of synthesis.

3.7. Experimental Section

FT-IR spectra were recorded using a JASCO FT/IR-6100 at room temperature under vacuum using a KBr pellet. Powder X-ray diffraction (pXRD) pattern of the electrochemically synthesized **NiDI** was obtained from Beamline BL44B2 ($\lambda = 1.08$ Å) at Super Photon ring-8 GeV (SPring-8) in Japan. The sample was ground finely packed into a 0.5 mm-diameter soda tube.

X-ray Photoelectron Spectroscopy data were obtained using PHI 5000 VersaProbe (ULVAC-PHI, INC.). Al Kα (15 kV, 25 W) was used as the X-ray source, and the beam was focused on a 100 μm^2 area. The spectra were analysed using the MultiPak Software and standardized using a C1s peak at 284.6 eV. Atomic Force Microscopy (AFM) was carried out using an Agilent Technologies 5500 Scanning Probe Microscope, under ambient conditions, in the high-amplitude mode (tapping mode), with silicon cantilever PPP-NCL (Nano World). PXRD simulations were calculated on CrystalDiffract program.

Cyclic voltammetry used a three-electrode configuration electrochemical cell with 1 M acetonitrile solution of tetrabutylammonium hexafluorophosphate as the electrolyte solution, a Pt coil as the counter electrode and an Ag^+/Ag electrode as the reference electrode. Their set ups were monitored by the 650DT electrochemical analyzers. (BAS Co., Ltd.) The reported potentials were adjusted from Ag^+/Ag to Fc^+/Fc using the difference in potentials between the two redox couples.

3.7.1. Synthesis of Nanosheets

Electrochemical synthesis of the **NiDI** nanosheets used a three-electrode configuration electrochemical cell with 1 M acetonitrile solution of Bu_4NClO_4 as the electrolyte solution, a Pt coil as the counter electrode and an Ag^+/Ag electrode as the reference electrode. Their set ups were monitored by the 650DT electrochemical analyzers. (BAS Co., Ltd.) The electrochemical polymerization was carried out on an indium-tin oxide (ITO) glass in a **HAB**·3HCl-Ni(OAc)$_2$-NH$_3$ aqueous solution with 0.1

M NaBF$_4$ as electrolyte under an argon atmosphere at a constant potential of 0.56 V vs. Ag/AgCl to oxidize the **HAB**. The black film on the ITO after applying the potential is the **NiDI** formed.

3.8.   References

1.   D. Herebian, E. Bothe, F. Neese, T. Weyhermüller, K. Wieghardt, *J. Am. Chem. Soc.*, **2003**, *125*, 9116-28.

Chapter 4

EXPANSION TO
OTHER METAL ION SYSTEMS

4 EXPANSION TO OTHER METAL ION SYSTEMS

This chapter is not published because it is scheduled to be published in journals or other publications within five years.

Chapter 5

CONCLUSION AND PERSPECTIVE

5.   CONCLUSION AND PERSPECTIVE

Using a bottom-up synthetic method, amino-based π-conjugated group 10 metal complex nanosheets were synthesized. These coordination nanosheets have been successfully synthesized using the hexaaminobenzene (**HAB**) ligand with optimized oxidation promoted interfacial reactions. This method, which was optimized based on the characteristic properties of the formation of a biradical during the synthesis of **NiDI**, has been proven to be applicable for the synthesis of other nanosheets such as the **PdDI**. This indicates a possibility that other similar 2D systems which involve oxidation can also utilize the new chemical or electrochemical methods to obtain large crystalline compounds for characterization ease or modified electrodes useful for measuring electrical properties.

In this dissertation, a few new CONASH systems have been investigated. Through the investigations of these systems formed, a variety of different physical properties of the each CONASH system have been found. Other than the electroconductivity in the semiconducting region, unexpected magnetic properties and a potential for charge storage applications have been found for the **NiDI** system. As for the **PdDI** system, a similar semiconductivity has been found, together with its memory effect which is the first time such effects have been found for 2D coordination compounds. This shows that even though these new CONASH systems are very similar in their structure and are all formed by group 10 metal ions, the resulting physical properties could be rather different, as observed by the lack of memory effect for **NiDI**.

These types of coordination nanosheets have proven to be rather intriguing, since many of their properties found can be yet to be fully explained. Furthermore, the bulk properties and the single or few layer samples could be very different as predicted from theoretical calculations. The latter, however, is difficult to achieve experimentally on a large scale with the current experimental method. As such, obtaining the monolayer or few-layer thick 2D materials is likely to be the one of the next goals for experimental research in this field. In this aspect, a combination of a bottom-up and top-down synthetic method could be considered. For example, after the formation of the

target compound by bottom-up synthesis, a top down method could be used to separate the sheets and obtain thinner or even monolayers of the target material.

Slight changes to the synthetic methods of these materials have also shown to cause some distinctive changes in their properties, such as in the case of **NiDI** when comparing the conductivity values found in this research and other research groups. It is plausible that by synthesizing them in a different way, the CONASH systems have slight structural differences and could be utilized differently in their applications. Further investigations could possibly shine a light into this relatively unknown terrain of these systems.

For the realm of 2D systems, much could be learnt from the graphene system, which is probably the best researched 2D system. Particularly for the modification of graphene for example, many graphene based materials have been modified to specifically tailor their properties for desired applications. This could probably also be applied to the CONASH systems which have been investigated in this dissertation. These systems also have pores present, which means a possibility of ion inclusion or trapping as an extension.

Although the permutations and combinations of metal and ligands to form coordination compounds seem to be endless, a couple of new 2D CONASH systems and their bulk properties have been thoroughly investigated in this dissertation. These discoveries pave the way for utilizing these systems in the future for plausible electronic or other storage devices.

APPENDIX

Appendix 1:

Ln (Resistivity) graphs of **NiDI**

LN(Resistivity) of NiDI 1

$y = 1.8941x + 0.324$
$R^2 = 0.9999$

LN(Resistivity)

(1000/T)(K^{-1})

LN(Resistivity) of NiDI 2

$y = 1.8661x + 0.5942$
$R^2 = 0.9998$

LN(Resistivity)

(1000/T)(K^{-1})
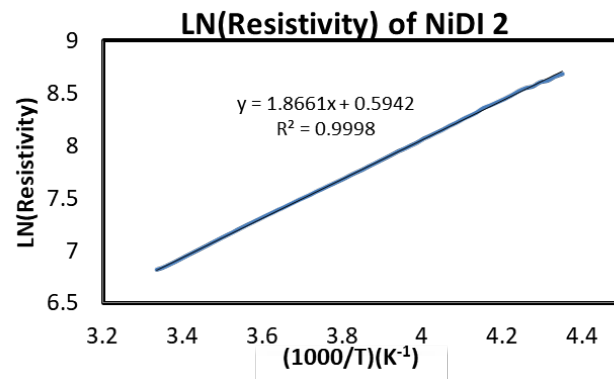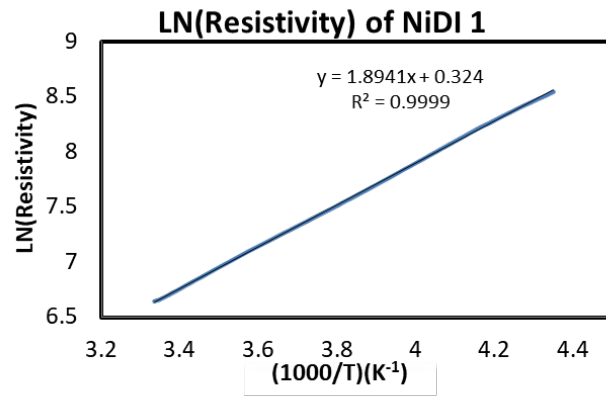
Appendix 2:

Conductivity data of another independent sample of **PdDI**

$y = 1.1256x - 0.7857$
$R^2 = 0.999$

$y = 2.5917x - 1.8091$
$R^2 = 0.999$
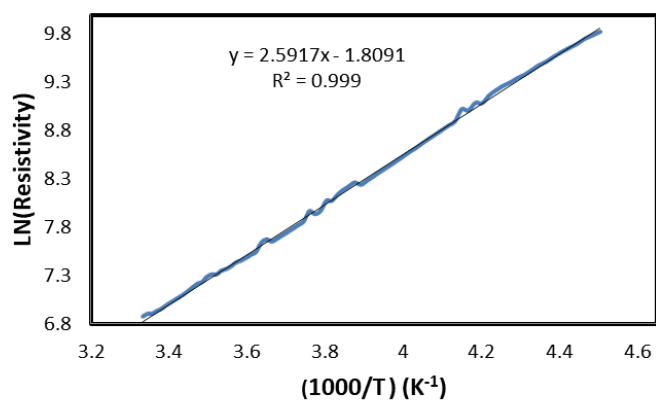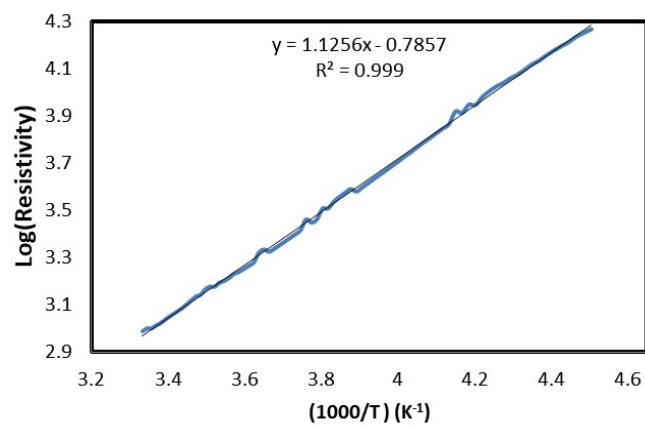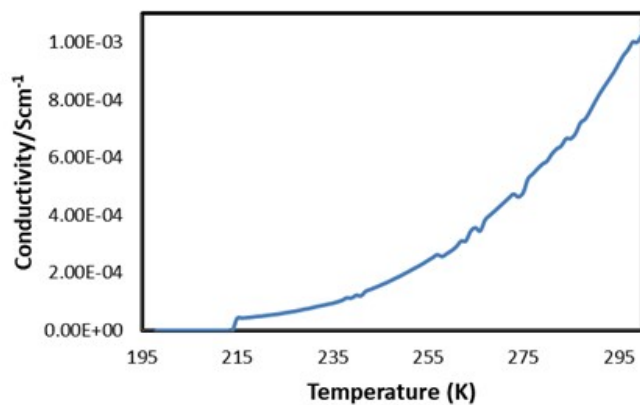
Appendix 3:

Ln (Resistivity) graph of **PdDI (**described in thesis)

LN(Resistivity) of PdDI

$y = 2.5442x - 1.8806$
$R^2 = 0.9993$

Y-axis: **LN(Resistivity)**

X-axis: **(1000/T) (K^{-1})**